

Copyright
by
Nicolas J. Huerta
2009

**The Thesis Committee for Nicolas J. Huerta
Certifies that this is the approved version of the following thesis:**

**Studying fluid leakage along a cemented wellbore: The sustained casing
pressure analogue, the influence of geomechanics and chemical
alteration on leakage pathway conductivity, and implications for CO₂
sequestration**

**APPROVED BY
SUPERVISING COMMITTEE:**

Supervisor:

Steven L. Bryant

Paul M. Bommer

**Studying fluid leakage along a cemented wellbore: The sustained casing
pressure analogue, the influence of geomechanics and chemical
alteration on leakage pathway conductivity, and implications for CO₂
sequestration**

by

Nicolas J. Huerta, B.S., M.S.

Thesis

Presented to the Faculty of the Graduate School of
The University of Texas at Austin
in Partial Fulfillment
of the Requirements
for the Degree of

Master of Science in Engineering

**The University of Texas at Austin
December, 2009**

Dedication

To Beth: Thanks for making the trip out to the 40 acres with me; I could not have done this without you.

Acknowledgements

I would like to thank Dr. Bryant for having faith that a geologist could become an engineer. Glen Baum, our experiment coordinator who is always helpful and infinitely patient when equipment seemed to fail at the worst moment. My undergraduate assistants Matt Li and Lauren Conrad, who took up the monotonous tasks with the enthusiasm of youth, your presence in the lab is already missed. My fellow graduate students, whose passion for learning is infectious. Dr. Bommer reading my thesis and teaching my first petroleum engineering course, the topic of production engineering is still one of my favorites. I am grateful to the sponsors of the Geologic CO₂ Storage Joint Industry Project at UT-Austin: BP, Chevron, ConocoPhillips, ExxonMobil, Foundation CMG, Halliburton/Landmark Graphics, Luminant, and Shell. Without their generosity and commitment to funding our research our work would not have been possible.

12/04/09

Abstract

Studying fluid leakage along a cemented wellbore: The sustained casing pressure analogue, the influence of geomechanics and chemical alteration on leakage pathway conductivity, and implications for CO₂ sequestration

Nicolas J. Huerta, M.S.E.

The University of Texas at Austin, 2009

Supervisor: Steven L. Bryant

Geologic storage of anthropogenic CO₂ remains the technology most likely to allow society to maintain current and future levels of energy production from fossil fuels and also reduce CO₂ emissions.

A key technological challenge for geologic storage is defining the probability of CO₂ leaks and estimating their impact. Leakage along faults and wells, whether they are pre-existing or created during operations, represent the most likely pathway by which CO₂ will leave the storage reservoir.

Understanding leakage along a well is an extremely complex problem due to the variability of well completions, pressure and temperature changes during the life of a

well, poor quantity and fidelity of well data, and the unknown fate of a well when subject to the environments expected during a CO₂ sequestration project.

This thesis considers two key aspects of well leakage (1) how to use an analog to estimate a well's leak path conductivity and (2) how leakage risk is affected by the coupling between pathway conductivity, cement alteration, and geomechanics in a well.

To address the first topic, a model of sustained casing pressure described in the literature (Xu and Wojtanowicz, 2001) is used to match observed pressure build up history on a well annulus. The effective permeability of cement is treated as the matching parameter. Results from case studies showed effective permeability values orders of magnitude larger than what is expected for intact cement. This strongly suggests that gas flows along distinct defects in the cemented annulus. The characteristic length for gas flow along several discrete pathways matched values from pathways generated in laboratory studies of zonal isolation. Such leakage paths respond differently to mechanical stress than a permeable matrix would. Thus an important implication of the sustained casing pressure analogue is that the geometry of the leakage pathway should be modeled explicitly, rather than treated as an equivalent permeable medium if one expects changes to the stress state around a wellbore or to the mechanical properties along the pathway.

To address the second idea we use core-scale experiments to quantify the coupling between flow and geomechanical stress along a cement/cement interface. The model flow channel is a fracture created by loading the sample according to the Brazilian method until it fails in tension. Using flow rate and pressure drop measurements we infer a fracture aperture. By cycling the confining stress we observe a reproducible relationship between confining stress and fracture aperture. This behavior is a function of the fracture geometry and mechanical properties of the cement. We then examine how

chemical alteration of the cement along the pathway can alter the flow/stress relationship. The observed change implies a fracture can be self-sealing to leakage of CO₂-saturated brine or of CO₂, although the exact mechanism, material plugging or cement strength decrease, remains unverified.

TABLE OF CONTENTS

ACKNOWLEDGEMENTS	v
ABSTRACT	vi
TABLE OF CONTENTS	ix
LIST OF TABLES	xi
LIST OF FIGURES	xii
CHAPTER 1 – INTRODUCTION.....	1
CHAPTER 2 – UTILIZING SUSTAINED CASING PRESSURE ANALOG TO PROVIDE PARAMETERS TO STUDY CO₂ LEAKAGE RATES ALONG A WELLBORE.....	6
SUMMARY.....	6
INTRODUCTION.....	7
MODEL SUMMARY.....	10
CASE STUDY 1.....	13
CASE STUDY 2.....	19
DISCUSSION.....	23
CONCLUSION.....	25

CHAPTER 3 – CEMENT CORE EXPERIMENTS WITH A CONDUCTIVE LEAKAGE PATHWAY, UNDER CONFINING STRESS AND ALTERATION OF CEMENT’S MECHANICAL PROPERTIES VIA A REACTIVE FLUID, AS AN ANALOG FOR CO₂ LEAKAGE SCENARIO.....	36
SUMMARY.....	36
INTRODUCTION.....	37
METHODS.....	40
RESULTS/DISCUSSION.....	47
CONCLUSIONS.....	50
CHAPTER 4 – THE INFLUENCE OF CONFINING STRESS AND CHEMICAL ALTERATION ON CONDUCTIVE PATHWAYS WITHIN WELLBORE CEMENT.....	60
SUMMARY.....	60
FRACTURE FLOW EXPERIMENTS.....	60
RESULTS/DISCUSSION.....	65
CONCLUSIONS.....	68
CHAPTER 5 – CONCLUSIONS.....	74
FUTURE WORK.....	75
REFERENCES.....	78
VITA.....	82

List of Tables

Table 2.1:	Key parameters used in the model.....	26
Table 2.2:	Leak depth and initial value parameters used in case study 1.....	26
Table 2.3:	Parameters for leakage geometry and leak source pressure from this paper and Xu (2002).....	27
Table 3.1:	D8 Results from core flooding.....	52
Table 4.1:	Schematic of the typical procedure used in our study.....	70
Table 4.2:	Experiment conditions for the two cores used in this study.....	70

List of Figures

Figure 1.1: Conceptual model for the key physics controlling long term leakage of CO ₂ up a wellbore.....	5
Figure 2.1: Well schematic with key geometric parameters labeled. Leak source is from some depth (D_L), gas flows up along cemented annulus (red arrow), and accumulates as pressure at the well head (P_g).....	28
Figure 2.2: Case study 1 well profile for our first case study (left). Pressure and temperature profiles are plotted versus total vertical depth (right). SCP is measured in the annulus between the production and intermediate casing.....	29
Figure 2.3: Case study 1 pressure history during bleed down, shut-in, and lubrication operations performed on the annulus. Four buildups were measured during shut in periods. Not shown is the final pressure reading of 4,200 psi which was recorded at 568 hr.....	30
Figure 2.4: <i>Buildup 1</i> . Leakage cannot be coming from depth A (casing seat at 10,607 ft TVD) because pressure cannot reach the recorded values. Plotted for the other depths are several different curves to illustrate the sensitivity of fits to different effective permeabilities.....	30
Figure 2.5: <i>Buildup 2</i> . Curves used in buildup 1 do not match the data for second buildup interval. Leakage from depth B is also ruled out because the final pressure is too low.....	31
Figure 2.6: <i>Buildup 3</i> . Previous fits do not match well here either because of the lower buildup rates. Fits from the deeper two locations are plausible when a lower permeability is used.....	31
Figure 2.7: <i>Buildup 4</i> . Previous curves (orange and purple) match well. Lack of long term pressure buildup data prevent us from identifying a leakage source depth based on this data alone.....	32

Figure 2.8: *Buildup 4*. Best fit (Depth D, $k=140$ mD) with long time pressure measurement.....32

Figure 2.9: This plot relates the best match permeability to the characteristic dimension of three equivalent geometries.....33

Figure 2.10: Long term pressure measurements on the intermediate annulus in case study 2. The stabilized pressure is estimated as 2,050 psi (green line), which is the average pressure from 10/02/04 to 01/02/05, excluding the single outlier.....33

Figure 2.11: Case study 2 wellbore schematic (right) showing relevant depths. Graph on left shows pressure and temperature gradients and interval of potential leak source.....34

Figure 2.12: Fitting results for four different depths for our second case study.....35

Figure 2.13: Plotted are the equivalent geometry for the annular area and range of effective permeability determined in case study 2.....35

Figure 3.1: Schematic diagram of cores with a conductive pathway and key geometries labeled. Image is of actual cement sample with conductive pathway caused by tensile failure.....53

Figure 3.2: The effective stress on a fracture causes deformation of the material at the asperities holding the fracture open. Increasing the effective stress reduces the average aperture of the fracture.....53

Figure 3.3: Pressure drop vs. pump volumetric flow rates for different aperture sizes. The blue vertical dashed lines represent upper limits for our pressure transducers (50 psi, 100 psi, and 500 psi). The horizontal blue lines represent our pump's flow rate range (0.01 ml/min to 9.99 ml/min).....54

Figure 3.4: How a small change in aperture size can be resolved with our current equipment setup. Solid lines are for indicated aperture size; dotted lines show effect of reducing aperture by 2 μm and dashed lines are for increasing aperture by 2 μm70

Figure 3.5: Three loading experiments for sawed and epoxied core at several flow rates (points within colored line) over a range of confining pressure. Each line represents a fixed confining pressure and its slope is related to the effective aperture of the fracture. In all experiments as confining pressure increases, the aperture size is decreased (yellow arrow).....56

Figure 3.6: Relation between aperture size and confining pressure for different incremental load experiments on sample B6.....57

Figure 3.7: Unreacted fractured cement cores show a characteristic decrease in aperture size as confining stress increases. The inlet pressure during the flow experiments is small, so the effective stress is approximately equal to the confining stress.....57

Figure 3.8: Before and after images of sample D8, which was subject to reaction with HCl.....58

Figure 3.9: Fractured cement cores reacted with acid (blue points) exhibit steeper trends of aperture vs. effective stress than unreacted cores (red points). The heavily reacted sample (blue triangles, Load Experiment 4) undergoes significant plastic deformation as the core is brought to the initial confining pressure of 50 psi. The acid reaction reduces the mechanical strength of the cement, allowing faster closure as confining stress increases.....59

Figure 4.1: Equipment setup. (Top Left) Fluid pump. (Top Right) Hassler cell used to hold the cement cores for fluid flow experiments under different confining pressures. (Bottom Right) Acid reaction setup consists of a glass dish to hold the acid and cement, a pH probe, and a stir plate. (Bottom Left) Close up of one half of cement core sitting with its fracture face exposed to acidic fluid.....69

Figure 4.2: (Left) Four flow rate experiments (colored lines), consisting of three flow tests (triangles) for each. Each experiment was conducted at a different confining pressure during the loading part of a cycle. The red arrow illustrates the trend of effective aperture size as confining pressure increases. (Right) Colored triangles show effective aperture obtained from corresponding confining pressure experiment. The black arrows indicate the direction of loading and unloading during our cycles.....70

Figure 4.3: The top left plot shows the baseline cycles for sample BB8. The top right shows the cycles after the core has been reacted with acid once. The bottom shows the strain hardened behavior developed in the baseline study is still present after the acid exposure.....71

Figure 4.4: The three images of on the left of the dividing red line are of sample F14B. The two on the right are of sample BB8. Note the significant (orange) color alteration across the fracture face in sample F14B after acid exposure. Also note that while sample BB8 was also exposed to acid, it was significantly less altered than sample F14B.....72

Figure 4.5: The aperture to confining pressure relationship for sample F14B. The baseline cycles are plotted as Cyc. 1-5 and the loading after the core was acidified is plotted as Acid. The acidified core behaves quite differently from the baseline study. While the acidified core starts out with an aperture comparable to those seen in the baseline study it quickly drops to a value much below those seen in the baseline cycles.....88

Figure 5.1: Initial results of flow through a fractured cement core using dilute hydrochloric acid. Note the channeling of flow through preferential pathways, which creates distinctly different reaction surfaces than we created with the uniform reaction technique.....77

CHAPTER 1 – INTRODUCTION

Geologic sequestration of anthropogenic CO₂ remains one of the most appealing technologies to reduce CO₂ emissions. This method would capture CO₂ from a point source, such as a coal fired power plant, and inject the fluid, ideally as a pure supercritical phase, into a geologic unit. This unit can be either a hydrocarbon bearing zone (either a depleted oil/gas reservoir or in association with enhanced oil recovery operations), deep saline aquifer, or unminable coal seam. While the petroleum industry has been moving fluids into and out of the earth for nearly a century, the magnitude of fluid to be injected, heterogeneity of the earth used to store and trap the CO₂, and need to verify that the CO₂ remains sequestered over a time scale perhaps longer than modern civilization makes this a daunting endeavor.

The U.S. Department of Energy and several industry consortia have provided the major funding toward initial development of this technology. There are currently several small scale pilot programs that are helping to develop or improve methods for site characterization, injection operations, plume monitoring, and leak detection. Moving forward from pilot scale studies to full deployment will require improvements in site selection methodology and the development of a complex system to capture, transport, and store the CO₂. A legal framework is also required to assign a monetary value to CO₂, permit site operations, and account for CO₂ stored. Most importantly, this technology must be perceived as both safe and necessary by the public for any sustained success.

Assuring secure storage of CO₂ is essential if we want to use carbon capture and storage (CCS) as a technology to reduce atmospheric CO₂. If CO₂ were to leak out of the storage volume it could reduce the value of overlying mineral or hydrocarbon resources, contaminate potable water, or return to the atmosphere. We need only to look at examples

such as Three Mile Island and the Yucca Mountain Repository to see how highly publicized accidents or the perception of risk can turn a populace against a technology. The challenge for CCS is then to understand the physical and geological phenomena of CO₂ storage, to quantify the risks, and to portray them to the stakeholders in a rational manner.

Wells and faults present the two most likely leakage pathways by which sequestered CO₂ can move out of the storage volume. Wells are especially important because they provide a direct and near vertical pathway through formations that otherwise act as a seal for CO₂. We must understand the following aspects of wells to begin to understand how to quantify leakage risk and impact. The exploration history of the area around or proximal to a candidate storage sites could be long and often poorly documented. Well completion requirements have changed throughout our nation's history and are typically regulated at the state level, which leads to different specific requirements and reporting protocol. Affecting the competence of all wells is the geology around the well, the well design, and well construction.

Oil and gas wells are known occasionally to fail to prevent migration of fluids between different subsurface formations, or between a subsurface formation and the surface. This unwanted migration can occur for numerous reasons and at different stages in the life of a well. During well construction the cemented annulus is especially prone to lose zonal isolation. Improper calculation and placement of cement can leave mud on the borehole wall or in the annulus or allow gas to channel through the setting cement. Later in life as the well is subject to different operations aimed at recovering more hydrocarbons, a leak can be created in the annulus. The cause can be pressure or temperature cycling or physical trauma to a well during work over operations. Once

detected, the petroleum industry has numerous methods to remediate the well and establish zonal isolation once again.

Despite the moderate probability of existing wells having some existing conductive pathway, monitoring of inactive or plugged wells may be minimal during CO₂ sequestration, and a leak might not be as easily detected as it is in oilfield operations. Regardless of whether leakage paths already exist, several phenomena during and after CO₂ sequestration can induce or exacerbate leakage. For example, during injection the geomechanical stress state around wells will change. The effect of increasing reservoir pressure on cement sheath integrity is unknown. Another factor is that cement reacts with both free phase CO₂ and with the carbonic acid that results when CO₂ dissolves into brine (Kutchko *et al.*, 2007). The reactions are slow but expected to occur over hundreds to a thousand years (Kutchko *et al.*, 2008). Moreover the coupling between geomechanics, fluid flow along some pathway in the well, and geochemical reaction of the pathway surface can lead to new behavior. During a sequestration project we expect significant pressure changes, first as the reservoir is elevated in pressure during injection and then as pressure returns to ambient levels after injection ends. The effects of pressure cycling on wells around the sequestration reservoir are unknown. If the fluid can communicate with a leakage path, elevated pore pressure might increase the size of the pathway. In typical oilfield operation a well would continue to leak, once a conductive pathway formed. A leaky well in a CO₂ storage operation could have CO₂-rich fluids reacting along the leakage conduit, thereby altering the mechanical properties of the material supporting the pathway. If this were to happen, then when the supporting pressure inside the pathway returns to background conditions, the pathway might seal. Fig. 1.1 summarizes the conceptual model of this coupling. To study the long term fate of a well we must develop quantitative understanding of how parameters couple. However quantitative

understanding of the parameters in an uncoupled fashion also has merit as we can use it to provide an initial estimate of leakage risk.

In lieu of actual field data from large scale CO₂ sequestration projects we can use analogs from the petroleum industry and laboratory experiments to forecast what might happen in and around the wellbore and what leakage rates to expect. The petroleum industry has a long history dealing with gas leaking up a cemented annulus (Bourgoyne *et al.*, 2000 and Watson and Bachu, 2007), which accumulates at the well top and is measured as pressure on the casing annulus. This is referred to as "sustained casing pressure" (SCP) or "surface casing vent flow." The petroleum industry typically focuses its efforts on prevention and remediation of the annulus pressure. However, some work has attempted to quantify leakage parameters, such as effective permeability and depth of gas leak (Wojtanowicz *et al.*, 2001). Since SCP data can be obtained from industry, we can use this approach to get estimates of conductivity of a failed cement sheath. Since the leakage pathway in SCP is analogous to the pathway that CO₂ may follow, we can estimate the pathway conductivity for CO₂ leakage. This parameter has been an *a priori* assumption in current approaches to estimating CO₂ leakage (Nordbotten *et al.*, 2005).

Laboratory experiments provide a means to incorporate aspects of the coupled system and isolate a few parameters to understand their relation. For example, we studied first how the conductivity of a pathway is affected by increasing the stress on a sample. We used this understanding as a basis to study the effect of geochemical reaction on the stress/conductivity relationship.

The technical content of this thesis is organized according to three conference papers. Chapter 2 is a paper presented at the 2009 Society of Petroleum Engineers' CO₂ Capture, Storage, and Utilization conference. This paper addresses modeling of sustained casing pressure to determine leakage parameters for wells leaking CO₂. Chapter 3 is a

CHAPTER 2 - UTILIZING SUSTAINED CASING PRESSURE ANALOG TO PROVIDE PARAMETERS TO STUDY CO₂ LEAKAGE RATES ALONG A WELLBORE

Summary

Predicting the flux of CO₂ along a leaking wellbore requires a model of fluid properties and of transport along the leakage pathway. This model should accurately represent the geometry of any discrete leakage pathway, because this geometry strongly affects the coupling between geochemical reactions and geomechanical response. Validating a transport model in advance of large-scale sequestration is difficult because instances of CO₂ plumes reaching abandoned wells are presently rare. However, natural gas leakage events along wellbores can provide insights into conductive pathways analogous to those anticipated for CO₂ sequestration. We apply a simple transport model to field measurements of sustained casing pressure (SCP) vs. time. We treat as unknowns the effective permeability of the leakage path and the depth at which leakage into the wellbore is occurring. These parameters are useful for forecasting likely leakage rates in sequestration sites located near oil and gas fields and for choosing candidate sites based on past exploration history. For several cases of SCP, conductive pathways (e.g. open fracture, gas channel, micro-annulus) must exist to explain the large inferred values of effective permeability. Applied to a large enough set of SCP wells, this approach can provide a probabilistic distribution of leakage rates given regional and well parameters. For CO₂ sequestration purposes this provides a tool to assess the risk associated with CO₂ migration along leaky wells, which is necessary for site selection, permitting, and properly crediting sequestration operations.

Introduction

The success of any geologic CO₂ sequestration operation depends on our ability to ensure that injected CO₂ is properly credited and that assets overlying the storage reservoir remain uncontaminated. To achieve both goals we need to verify that CO₂ does not leak out of the target formation at a rate large enough to adversely affect other compartments of economic or environmental value. A physics-based model for leakage will be a valuable tool for assessing risks associated with a prospective storage project and for analyzing field observations.

The most probable pathways for leakage are faults and wells. Wells conceivably provide a direct path to shallower subsurface formations and to the surface. Their geometry and their sealing capability are highly variable. The petroleum industry has extensive experience with leaky wells. In some of these wells, the leakage path involves a cement/steel interface (typically a micro-annulus) and/or a conduit within the cement (gas channel or fractures). If the leakage path terminates at a sealed wellhead, then pressure will be sustained in the casing annulus. In contrast, the leakage path of primary concern in CO₂ sequestration continues outside the casing.

The similarity between gas leakage and CO₂ migration is in the leakage pathway. Conduits within cement should behave in essentially the same way in both cases. The cement/steel interface relevant to gas well leakage differs in some important ways from the cement/earth interface relevant to CO₂ migration. Nevertheless we expect the effective permeabilities of the two types of interface to be of similar magnitude. Thus by studying the nature of leakage pathways in oil and gas wells, we can estimate the range of leakage rates likely to occur in a CO₂ sequestration operation.

WELL GEOMETRY

Construction of each well is a unique event both in terms of planning and implementation. However, all wells share some common features and must perform certain functions. A typical well completion has several strings of casing cemented in place over some interval (Fig. 2.1). The key functions of a cemented annulus are to provide support for the weight of the casing, protect the steel casing from corrosive fluids, and isolate geologic zones with respect to fluid migration (Nelson and Guillot, 2006). Loss of zonal isolation can lead to contamination of overlying aquifers or loss of hydrocarbon resources. Gas migration into shallow formations or accumulation to significant pressure under a wellhead could create a health and safety hazard.

REASONS FOR SUSTAINED CASING PRESSURE

Sustained casing pressure (SCP) refers to buildup of pressure due to a flux of fluid into a well's annulus. SCP connotes a significant and persistent buildup of pressure over time, as opposed to a small fluctuation in annulus pressure associated with temperature changes in the well. Unfortunately the occurrence of SCP is not rare. A report on wells in the outer continental shelf (OCS) for the Minerals Management Service (MMS) (Bourgoyne *et al.*, 2000) showed numerous instances of pressure buildup on the annulus. Of the 8,000 wells surveyed on OCS, 11,000 casing strings (each well had multiple casing strings) exhibited sustained casing pressure. The most common type of leak occurs through tubing or casing failure and is typically easier to remediate than the annular leakage that is the focus of this paper. The report also showed that the most significant cause of SCP on casing strings outside the production casing was caused by poor cement bond (Bourgoyne *et al.*, 2000). Indeed SCP is not limited to offshore wells; a survey paper by Watson (2007) showed significant instances in the oil and gas province of Alberta. She found that 4.5% of the 315,000 wells on record failed to prevent surface

casing vent flow (equivalent to SCP) or exhibited gas migration through the soil (Watson, 2007). These statistics seem to indicate a higher rate of offshore well integrity issues. Since the cost of offshore well remediation is so prohibitively expensive, unless wellbore integrity is better prevented or remediation methods improved offshore CO₂ sequestration might not be an option. For land based wells, Watson (2007) found that the cause, geometry, time of occurrence, and severity of a failed cement annulus do show some correlations. While not exclusive, the factors can be categorized into two distinct time scales.

SHORT TERM EFFECTS

Short term effects are related to operations during well completion but before stimulation, fracturing, or acid jobs are performed. Pressure exerted by mud and cement column could be too close to the hydrostatic pressure thus allowing gas to infiltrate the cement when it is setting. Borehole rugosity and poor casing centralization can contribute to poor mud displacement and/or mud being left on the borehole wall. Cement-related events are also commonly to blame for early stage SCP. For example, many problems are created if the cement formulation allows excessive fluid loss to the formation. If the cement is not allowed to develop adequate strength before further drilling, cement integrity at the casing shoe might fail. The most typical short term effect is the creation of channels filled with gas or mud.

MEDIUM TO LONG TERM EFFECTS

Medium to long term effects are related to completion and operation of the well. Typical operations involve pressure or temperature cycling along the wellbore which could expand casing and lead to detachment between the steel (elastic) and cement (brittle) interface. Cement can also be stressed from internal deformation to a point that it

fails and tensile cracks form. Normal pressure decline of a formation can lead to an altered stress state around the wellbore. Typical results from longer term effects are micro annulus or micro fractures in the cement.

Experimental studies of conductive pathways have been performed to demonstrate new cement formulations or novel well logging techniques. One set of experiments created micro annuli with effective permeability ranging from 0.1 mD to 100 mD after successive loading and unloading events in conventional neat cement (Boukhelifa et al., 2005). Another study created micro annuli with 1 μm to 1 mm separation between cement and casing. The effect of fluid (water or gas) within the micro annuli on sonic and ultrasonic well logging instruments was then examined (Jutten and Hayman, 1993). Modeling efforts are frequently conducted to study geomechanical phenomena that cause a loss in zonal isolation or to help develop procedures to achieve a successful cement job. Conductive pathways created in such models are typically on the order of 10 μm (Gray et al., 2007). Importantly, leakage in an annulus is not expected through the cement matrix. Intact cement has permeability on the order of 0.01 mD to 0.001 mD. Persistent pressure buildup is thus associated with flow through a discrete, conductive pathway of the types described above.

Model Summary

The mathematical model of pressure buildup used here was developed from a series of studies to investigate sustained casing pressure in the OCS (Wojtanowicz *et al.*, 2001). Given the basic geometry of the well construction, the model computes a buildup curve (pressure versus time). The user can adjust parameters such as effective permeability of the cement to fit pressure data recorded at the casing head (Xu and Wojtanowicz, 2001; Xu, 2002). The model treats the leakage path as a Darcy-flow

continuum, rather than a discrete pathway. Despite this simplification, the model yields useful estimates of the magnitude of effective permeability.

MODEL ASSUMPTIONS

This model assumes a liquid column (typically mud) above the cemented interval in an annulus. It assumes the leakage path is one dimensional with length equal to the length of cement and that gas flows along it according to Darcy's law. The driving force for the flow is the difference between the (constant) pressure at the leakage depth (P_L) and the pressure at the top of the cement. The latter is the sum of the pressure from the mud column weight (P_m) and the accumulated gas pressure (P_g).

Buoyancy is ignored and gas density is assumed proportional to pressure (constant Z and gas viscosity). The buildup is computed by assuming steady state flow during each step in a series of short time steps. Between steps, gas accumulates and pressure at the top of cement increases, reducing the driving force for leakage. Flow through the mud/liquid-filled portion of the annulus is assumed instantaneous. Mud is assumed slightly compressible so that its volume decreases as pressure builds in the annulus. The steel casings bounding the annulus are treated as incompressible. When the sum of casing and mud pressure is equal to leak formation pressure, gas flow ceases.

KEY PARAMETERS AND THEIR EFFECT

Key parameters are listed on Table 2.1 and shown schematically on Fig. 2.1 where possible. Standard pressure and temperature are 14.7 psi and 32 °F respectively. The gas is assumed to be at an average wellbore temperature, computed from temperature at the leakage depth and the temperature at the wellhead. The annulus area is calculated from the outer diameter of the inner casing to the inner diameter of the outer casing. The two main features of the buildup are its curvature and the final (maximum) value of

pressure. For most applications we treat the depth and pressure at the leakage point and the effective permeability of the leakage path as unknown fitting parameters, adjusting their values until the model buildup curve is close to the observed pressure buildup. For other parameters that are poorly constrained, it is important to know what feature of the curve they affect and how sensitive the curve is to their variability.

Stabilized Buildup Pressure

Parameters that affect final pressure are: formation pressure (the pressure at the leak source), mud length and mud density. Typically, regional pressure gradient or well-specific pressure measurements at some depth are used to correlate formation pressure to a potential leak depth. An increase in mud density and a longer mud-filled annulus will lead to a lower stabilized pressure.

Pressure Buildup Rate

Pressure buildup rate is controlled by size of gas chamber above mud, length of mud column, mud compressibility, and cement's effective permeability. Mud column length is typically known from the well completion geometry. Gas chamber length can be estimated from the type of fluid produced during an annulus bleed down. If there was no liquid then we assume there is a significant void space at the top of the annulus. The rate of pressure buildup decreases as the length of gas or mud increases. Mud compressibility is easy to measure but rarely collected (Xu and Wojtanowicz, 2001). Hence we use an empirical correlation based on mud density and type of fluid (Kutasov, 1988). Higher mud compressibility leads to a slower pressure buildup, though the model is only sensitive to mud compressibility in wells with a long mud column.

Case Study 1

SUMMARY OF SCP HISTORY

The first case study comes from an onshore gas well in an over-pressured reservoir (0.92 psi/ft). Soon after cementing the production casing, the annulus between production and intermediate casings began to exhibit SCP (Fig. 2.2). Pressure buildup was several thousand psi within one day. After bleeding of gas entrained in the mud several times, the operating company lubricated the annulus (injected high density mud to increase the weight on cement and displace gas from the mud). SCP occurred after each of these operations. Though unwelcome for the operator, the series of SCP measurements allows us to estimate effective permeability of the leakage path and the depth to the leakage point. Not shown in Fig. 2.3 is a later, long-term buildup, during which the annulus pressure stabilized at 4,200 psi. Eventually the well was perforated and operators attempted a squeeze job that was only temporarily successful. Our analysis provides an explanation for this failure and is discussed below.

DESCRIPTION OF MODEL PARAMETERS

Cement Permeability

The effective permeability of the cement is expected to be large because pressure buildup is rapid. Because the SCP occurred soon after the cementing operation, the likely leakage path is a channel in the annulus caused by poor mud displacement or gas invasion into the wellbore. The model does not account explicitly for the geometry of the leakage path. We will interpret the effective permeability inferred from the model in terms of the equivalent aperture of a conduit for leakage.

Leakage Depth

Based on the well design, the most likely location for the leak was the interval between the well bottom (13,171 ft TVD) and the 7" casing seat (10,607 ft TVD). Along this interval the cement in the annulus between the production and intermediate casing contacts the borehole wall (Fig. 2.2). We considered several locations along the interval that targeted specific weak points in a well. Depth A (10,607 ft TVD) was chosen because a cement job often fails at the casing seat. Depths B (11,470 ft TVD) and C (11,934 ft TVD) give a good spread over the potential leakage interval. Depth D (13,059 ft TVD) was chosen based on calculating the leak pressure that would equal the sum of the pressure from the mud and accumulated gas with pressure of 4,200 psi. The latter value is significant because it was measured weeks after the cementing operation and is our best estimate of stabilized annulus pressure.

The calculation of depth D is shown below. The stabilized pressure occurs when there is no pressure drop along the leakage path through the cement, i.e.

$$P_L - (P_m + P_g) = 0 \quad (2.1)$$

$$P_g = 4,200 \text{ psi} \quad (2.2)$$

Mud pressure (P_m) is given by:

$$P_m = \frac{\rho_m g L_m}{g_c} = \frac{17.39 \frac{\text{lbm}}{\text{gal}} \times \frac{1 \text{ gal}}{0.134 \text{ ft}^3} \times \frac{1 \text{ ft}^2}{144 \text{ in}^2} \times 32.2 \frac{\text{ft}}{\text{s}^2} \times 8,700 \text{ ft}}{32.2 \frac{\text{lbm} \cdot \text{ft}}{\text{lbf} \cdot \text{s}^2}} = 7,841 \text{ psi} \quad (2.3)$$

where ρ_m is the mud density, g is gravity, L_m is the mud column length, and g_c is a conversion factor between pounds mass and pounds force.

Our leak pressure (P_L) is related to leakage depth (D_L) by:

$$P_L = 0.92 \frac{\text{psi}}{\text{ft}} \times D_L \quad (2.4)$$

Combining Eqs. 2.2, 2.3, and 2.4 with Eq. 2.1 and rearranging to solve for leakage depth gives:

$$D_L = \frac{4,200 \text{ psi} + 7,841 \text{ psi}}{0.92 \frac{\text{psi}}{\text{ft}}} = 13,059 \text{ ft} \quad (2.5)$$

The corresponding pressure at that depth is:

$$P_L = 0.92 \frac{\text{psi}}{\text{ft}} \times 13,059 \text{ ft} = 12,041 \text{ psi} \quad (2.6)$$

Temperatures

A temperature log was acquired near the time that SCP was measured and is used to determine temperatures at both the leak depth and the well head (Fig. 2.2).

Pressures

The two key pressures are pressure at the leak location and initial pressure for the SCP build up. Pressure at the leak was calculated based on the operator provided pressure gradients for the area (0.433 psi/ft above 11,000ft and 0.92 psi/ft below). Three pressure readings at the perforations validated our pressure profile (Fig. 2.2 – Three red dots). Depth A was close to the transition zone between pressure gradients but we used the higher gradient to allow for a larger pressure buildup. The first pressure value for each buildup was used for the initial pressure value in the fit. Table 2.2 shows pressures for each depth and buildup.

Casing Diameters

The operators used 4.5", 15.1 lb/ft P-110 for the production casing with outer diameter of 4.5". The intermediate casing was 7", 29 lb/ft P-110 which has an inner diameter of 6.184". We ignore the effects of borehole rugosity in the zone below intermediate casing seat and assume a uniform (6.184") cross sectional area throughout the annulus length.

Mud and Gas Column Lengths

Mud column length was taken from top of cement to the surface. The drilling report showed that a small amount of gas was bled before producing mud, so we assume the initial gas column length to be negligible.

Mud Density and Compressibility

Mud density was tracked during bleed downs, build ups, and annulus lubrications. For the first two buildups mud density was 17 lb/gal. For the second two buildups we used 17.39 lb/gal. The increase in density was due to attempts by the operator to lubricate with kill fluid (20 lb/gal). Compressibility of mud was taken as 3.0×10^{-6} psi⁻¹ (Kutasov, 1988).

Gas Properties

We estimate gas deviation factor to be 0.86 and viscosity to be 0.02 cp, using the T and P of the well and a natural gas lookup table (McCain, 1990). Since the composition of the gas was unknown we varied these parameters in our preliminary calculations and found they had a relatively minor effect on the buildup curves.

RESULTS AND DISCUSSION OF PARAMETER FITTING

We fit the data with permeability values for each of the four proposed leak sources to determine leak source. The intermediate casing seat location (depth A) gave an unsatisfactory fit for any permeability, because the stabilized buildup pressure was too low (Fig. 2.4 – light blue line). The best visual fits for the other three depths are the maroon curve (depth B, $k=1,000$ mD), orange curve (depth C, $k=750$ mD), and light green curve (depth D, $k=350$ mD). Next, we compare these curves to buildup data 2.

The previous best fits applied to buildup 2 overestimate initial rise in pressure (Fig. 2.5). For each depth, we decreased permeability to account for the slower buildup rate. Only depth C and D were able to adequately match later data points. The fit using depth B did not match late time data and was eliminated as the leakage source. The best fit permeabilities for buildup 2 were approximately half the values used for buildup 1. The two best fits were depth C, $k=500$ mD (blue curve) and depth D, $k=300$ mD (violet curve).

The best fits from buildup 2 overestimate the early time pressure of buildup 3 (Fig. 2.6). Smaller permeability for both locations once again yield close matches. Determining which leak depth (depth C, $k=200$ mD or depth D, $k=150$ mD) gave a better fit was not possible because of sparse early measurements and no long term buildup data.

Two best fits from the previous analysis match buildup 4 data (Fig. 2.7). Buildup behavior was insensitive to small changes in permeability (e.g. depth D, $k=140$ mD versus $k=150$ mD). Additionally, leakage from both depths had similar behavior across buildup 4 data. Based on this alone, we would not be able to resolve leakage depth beyond bounding it between C and D. However, the completion report showed 4,200 psi on the intermediate annulus three weeks after the last pressure reading on Fig. 2.2. Leak depth D was chosen to match the long term pressure and using effective permeability of $k=140$ mD not only matches early buildup behavior but reaches a stabilized pressure of 4,200 psi within three weeks (Fig. 2.8).

A deep leak might explain why the operator's initial efforts to squeeze cement around 8,483 ft TVD did not yield successful long term zonal isolation. The source of the leak was actually much lower and would still exert significant pressure on the remedial cement job. We attribute the progressive drop in buildup rate to excessive gas in the mud being expelled from the annulus during bleed off operations. The flow of gas into the

mud column before cementing would have been quicker than after the cement had gelled – leading to a higher apparent flux of gas in the early buildups. While permeability drops significantly in the first few buildups, it stabilizes in the final two buildups. The key point is that while permeability for the buildups varies, all the values are orders of magnitude higher than plausible for intact cement. Therefore, a discrete conductive pathway such as a micro annulus or a gas channel must be the conduit for gas flow.

EQUIVALENT GEOMETRY

The dimension of discrete pathways can be calculated using, for a gas channel, the Hagen-Poiseuille equation. The product of the annular area (A) and effective permeability (k) in Darcy’s law must correspond to the geometric term in the Hagen-Poiseuille equation:

$$kA = \frac{\pi R^4}{8} \quad (2.7)$$

where R is the radius of the gas channel.

Similarly, for flow through a micro fracture or micro annulus the slit-flow equation is applicable:

$$kA = \frac{WB^3}{12} \quad (2.8)$$

Here W is the distance between casings (micro fracture) or inner casing circumference (micro annulus) and B is the aperture (micro fracture) or separation between casing and cement (micro annulus).

Permeability versus leakage geometry for the annular area in this case study is plotted in Fig. 2.9. The best fit permeability is indicated by the vertical black line. The effective permeability corresponds to characteristic sizes of 238 μm for a channel, 92 μm for a micro fracture, and 23 μm for a micro annulus. These sizes fall within the range of geometries created in laboratory studies reported in the literature.

Case Study 2

SUMMARY OF SCP HISTORY

Our second case study is from an onshore sour gas well in Alberta. Sustained casing pressure was evident in both production and intermediate annulus. Compositional analysis of gas recovered from the production tubing, production annulus, and intermediate annulus were distinct, and thus inferred to be from different sources¹. Leak pathways in each annulus were confirmed as isolated based on an integrity test that showed no pressure communication between the production and intermediate annulus¹. To perform the SCP analysis we use pressure data on the intermediate annulus (Fig. 2.10) from before the pressure integrity test as an estimate of the maximum stabilized pressure (2,050 psi) and for the buildup we use data collected after the integrity test. Well construction data (Fig. 2.11) showed that the intermediate annulus had a two stage cement job which failed because the stage collar was open during both stages. The operators performed remedial cementing at the casing shoe by perforating and circulating slurry to attempt to cement the shoe in place. They also performed several cement squeeze jobs at the stage collar and remedial perforations because they were not holding pressure. Eventually the annulus held sufficient pressure to continue with drilling operations but later began to exhibit SCP.

DESCRIPTION OF MODEL PARAMETERS

Cement Permeability and Top of Cement

Due to the numerous cementing operations the condition of the cement and how well it displaced the mud originally in the annulus is unknown but must surely be poorly

¹ Personal communication with T. Watson. 2009. Calgary: T.L. Watson & Assocs. Inc.

and unevenly distributed. Based on the numerous remedial cement jobs we assume there is some continuity of cement from the casing shoe at least up to the stage collar. During the second stage of the cement job the operators reported returns to surface, however the more dense cement slurry must have displaced the lighter mud and settled to some depth below the wellhead before setting. Top of cement can be related to leakage depth and length of mud column if we know mud density, hydrostatic gradient, and the stabilized annulus pressure as we show below.

Leakage Depth

Leakage depth is unknown, and several different points along the well will be studied. The source must be from above the intermediate casing shoe (7,392 ft) and below the production casing shoe (1,517 ft). We can restrict the upper boundary for the leak to the point where hydrostatic pressure is equal to stable pressure measured on the annulus. This minimum leakage depth is calculated based on a pressure gradient of 0.433 psi/ft and stabilized pressure of 2,050 psi. From the pressure balance of the model we have at stabilized pressure:

$$P_L - (P_m + P_g) = 0 \tag{2.9}$$

$$P_L = 0.433 \frac{psi}{ft} D_L \tag{2.10}$$

$$P_g = 2,050 psi \tag{2.11}$$

Assuming no mud ($P_m = 0$) and solving for leak depth we have:

$$\frac{2,050 psi}{0.433 \frac{psi}{ft}} = 4,734 ft \tag{2.12}$$

This assessment narrows the possible leak depth to the interval between 4,734 ft and 7,392 ft TVD.

Temperatures

The bottom hole temperature reading was 239 °F (at 11,991 ft TVD) and the surface temperature reading was 36 °F, measured at the start of the pressure buildup. The temperature gradient between these two measurements is 17 °F/1,000 ft (Fig. 2.11).

Pressures

Pressure gradient is unknown. Bottom hole pressure was estimated on the well completion diagram to be 4,931 psi (at 11,991 ft TVD). At this depth the corresponding pressure gradient would be less than hydrostatic, possibly because the target reservoir had been in production for several decades. We use hydrostatic gradient of 0.433 psi/ft to estimate pressure at leakage depth (Fig. 2.11).

Casing Diameters

The intermediate annulus is 9 5/8" N-80 53.50 lb/ft with an inner diameter of 8.535". The surface casing is K-55 13 3/8" 68 lb/ft with an inner diameter of 12.415".

Gas Properties

Gas composition was collected from the production tubing, production annulus, and intermediate annulus. We used a PVT simulator with the gas composition to estimate the mean gas properties along the depth of interest in our well (gas deviation factor of 0.92 and viscosity of 0.015 cp).

Mud Density and Compressibility

Mud density was given as 10.1 lb/gal. The mud is an oil based mud and using an empirical correlation we set the mud compressibility to $6.5 \times 10^{-6} \text{ psi}^{-1}$ (Kutasov, 1988).

Mud and Gas Column Lengths

Lengths of the mud and gas columns in the annulus are unknown. During bleed down of the intermediate annulus gas and oil based mud were recovered. We assume length of gas to be negligible during the start of buildup as the same volume of fluid recovered during the bleed was lubricated back into the well. Mud length is estimated at a given leak depth based on the model's pressure balance equation. Knowing some key parameters, we derive the relationship below.

$$P_L - (P_m + P_g) = 0 \quad (2.13)$$

Irrespective of leak depth the maximum pressure at the surface is:

$$P_g = 2,050 \text{ psi} \quad (2.14)$$

Pressure at the leak is defined by picking a leak depth and using the following pressure gradient:

$$P_L = 0.433 \frac{\text{psi}}{\text{ft}} D_L \quad (2.15)$$

Pressure of mud is a function of the density of mud and length of mud column:

$$P_m = \frac{\rho_m g L_m}{g_c} = 0.523 \frac{\text{psi}}{\text{ft}} L_m \quad (2.16)$$

Plugging in the relations and simplifying we get

$$0.433 \frac{\text{psi}}{\text{ft}} D_L - \left(0.523 \frac{\text{psi}}{\text{ft}} L_m + 2,050 \text{ psi} \right) = 0 \quad (2.17)$$

Solving for length of mud gives

$$L_m = \frac{0.433 \frac{\text{psi}}{\text{ft}} D_L - 2,050 \text{ psi}}{0.523 \frac{\text{psi}}{\text{ft}}} \quad (2.18)$$

Thus for the potential leakage depth there is a corresponding length of mud, which is bounded by no mud ($D_L = 4,734$ ft) and 2,200 ft of mud ($D_L = 7,392$ ft).

RESULTS AND DISCUSSION OF PARAMETER FITTING

For a given leak depth in the interval examined, effective permeability and initial gas length were varied to match early and later buildup data. Leakage depth could not be uniquely determined because a combination of gas length and permeability seemed to allow an adequate fit (Fig. 2.12). However, it takes a longer gas length to achieve a good fit with a deeper leak source, especially for the early time behavior (Fig. 2.12 blue curve versus green curve). Information from well operations implies that a significant gas length is not present therefore a deep leak depth is less likely. However to model early time behavior at any depth some length of gas is needed; a length of 2 ft seemed to match the shallow leakage depths. Permeability needed to fit the model decreased with depth and increased with gas length used. Permeability between 0.1 mD and 5 mD matched all depths and all reasonable gas lengths.

EQUIVALENT GEOMETRY

Because a range of fairly large permeabilities provide an adequate fit, the size of potential leakage pathways is correspondingly large (Fig. 2.13). For a gas channel we have 53 μm to 140 μm , for a micro fracture we have 10 μm to 38 μm , and for a micro annulus we have 2 μm to 9 μm .

Discussion

The SCP model applied to the first case study showed a significant leak at depth best interpreted as a discrete pathway. Wells that experience a large flux of gas early on are more likely to have pathways due to gas channeling or poor mud displacement and than to have micro annulus fractures or debonding associated with pressure and temperature cycling. Limited input data forced us to estimate a range of leakage geometry for the second case study but the size still falls within realistic bounds. Further case

studies that have high resolution data and an independent means to verify leakage depth would allow us to make a more precise determination of leakage pathway geometry.

Data on wells with SCP sufficient to model the leakage pathway are relatively rare and might be unavailable in a candidate sequestration area. However more general wellbore information is typically available from a government agency (e.g. Texas Railroad Commission or Alberta Energy and Utilities Board). Ideally we would relate leakage parameters from case studies, as shown in Table 2.3, to more readily available well information (such as age, depth, geometry, production history). For example, the effective permeabilities (Table 2.3) determined for the wells originally studied by Xu (2002) might be indicative of values from offshore wells. Or perhaps the reason case study one has a much higher effective permeability when compared to case study two is related to the overpressure seen in case study one as compared to the hydrostatic gradient in two. By correlating wellbore information with leakage parameters in a probabilistic approach (Watson and Bachu, 2008) we can advance models from simply predicting leakage to estimate potential leakage rates for the area.

To properly address the long term fate of CO₂ a more robust model than the one used here needs to be developed. This model should take into account the physical properties of CO₂ as it moves out of the storage formation. It should also treat transport along the wellbore using a discrete pathway. This approach is key for modeling CO₂ leakage along a well because we must also consider the effect of chemical alteration of cement by CO₂ and the effects of geomechanical stresses on the wellbore. Cement is reactive with CO₂ and CO₂-saturated brine (Kutchko *et al.*, 2007), and the coupling between reaction and geomechanical stresses influences the geometry of the leakage pathway (Huerta *et al.*, 2008).

Conclusion

Wells that exhibit sustained casing pressure due to migration of natural gas are a useful analog for quantifying the potential magnitude of CO₂ leakage along a wellbore. We implemented Xu's model (Xu and Wojtanowicz, 2001) of the pressure-driven migration of gas through cement into a closed annulus. Application of the model to two examples of field data yields information about depth of leak and effective permeability of the cement. The effective permeability was about 140 mD for one well, and was in the range 0.1 mD to 5 mD for the other well. These values are two to four factors of ten larger than the permeability of intact cement. Thus we convert values of effective permeability into equivalent geometry of a discrete leakage pathway, such as a gas channel, micro fracture, or micro annulus. These values are useful in understanding potential leakage rates of CO₂ along a wellbore because CO₂ moving along the leakage path will react with the cement. The reaction alters the mechanical properties of the cement. The geomechanical stress can thus alter the geometry of the leakage path. Applying the model presented here to other wells can indicate the likely range of apertures for leakage pathways. The model must be extended to handle CO₂ phase behavior and geochemical/geomechanical coupling before it can assess longer-term CO₂ leakage rates along a wellbore.

Table 2.1—Key parameters used in the model

Parameter	Units	Symbol
Temperature at leakage depth	F (K)	T_L
Wellhead temperature	F (K)	T_{wh}
Outer diameter of inner casing string	in (m)	D_1
Inner diameter of outer casing string	in (m)	D_2
Cement length	ft (m)	L_c
Initial mud length	ft (m)	L_m
Initial gas length	ft (m)	L_g
Gas viscosity	cp (Pa*s)	μ_g
Mud compressibility	psi ⁻¹ (Pa ⁻¹)	c_m
Mud density	lbm*gal ⁻¹ (kg*m ⁻³)	P_m
Gas deviation factor	-	Z
Effective permeability	md (m ²)	k
Pressure at leak source	psi (Pa)	P_L
Annulus Pressure at well head	psi (Pa)	P_g

Table 2.2—Leak depth and initial value parameters used in case study 1

Pressure at Leakage Depth, psi	
A	9,758
B	10,552
C	10,978
D	12,041
Initial Pressure for Each Buildup, psi	
1	0
2	0
3	1,250
4	1,000

Table 2.3—Parameters for leakage geometry and leak source pressure from this paper and Xu (2002)

Case Study	Effective Permeability, mD	Channel Radius, μm	Micro Fracture Aperture, μm	Micro Annulus Gap, μm	Leak Source Pressure, psi
Case 1	140	238	92	23	12,015
Case 2	0.1 to 5	53 to 140	10 to 38	2 to 9	2,050 to 3,200
Well 23 (Xu, 2002)	0.403	71	15	4	6,515
Well 24 (Xu, 2002)	0.94	84	20	5	6,330

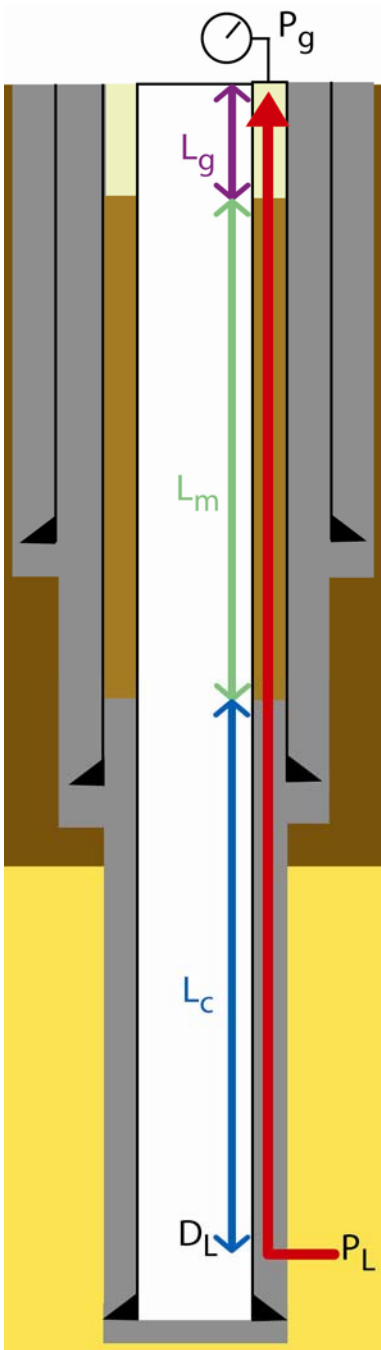


Fig. 2.1—Well schematic with key geometric parameters labeled. Leak source is from some depth (D_L), gas flows up along cemented annulus (red arrow), and accumulates as pressure at the well head (P_g).

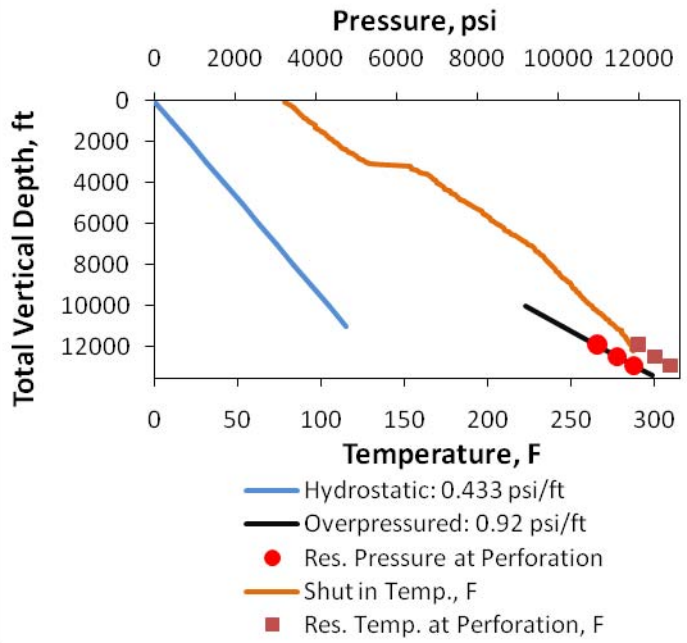
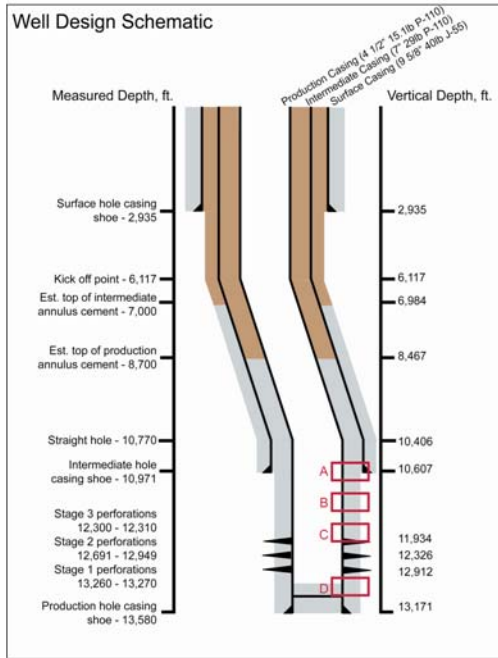


Fig. 2.2—Case study 1 well profile for our first case study (left). Pressure and temperature profiles are plotted versus total vertical depth (right). SCP is measured in the annulus between the production and intermediate casing.

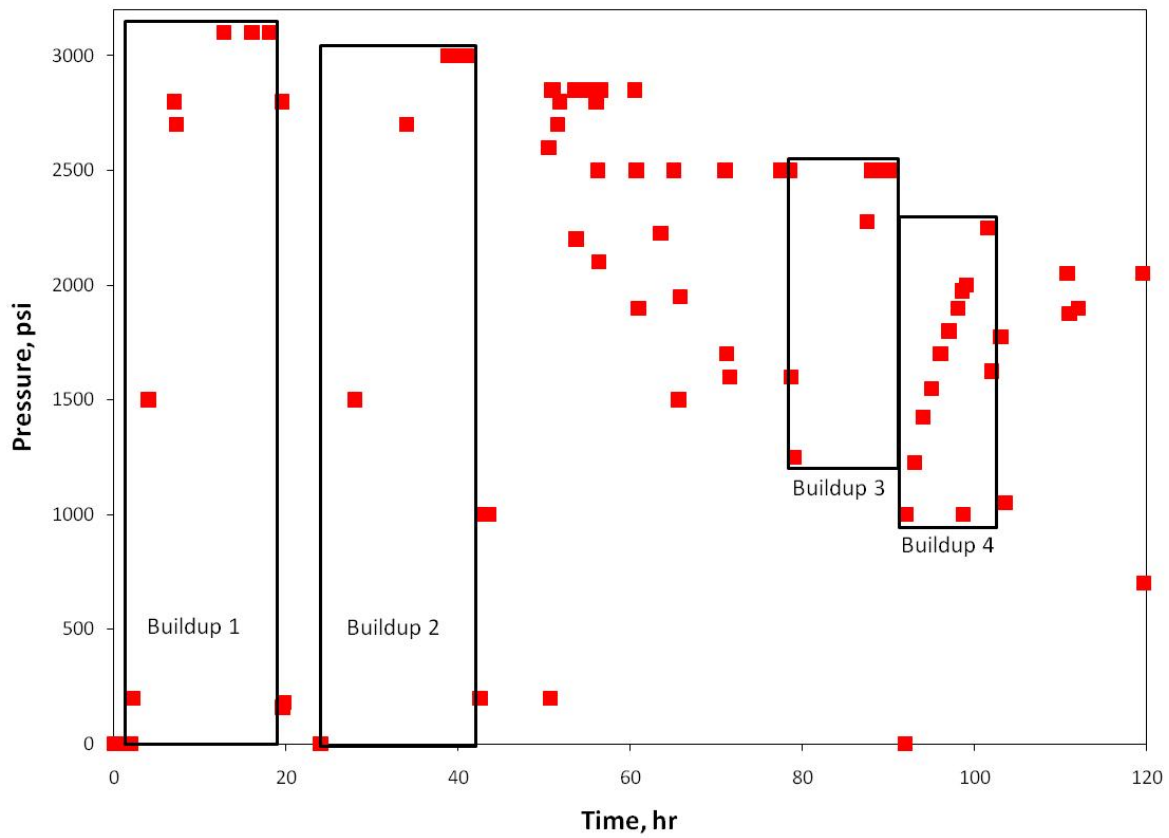


Fig. 2.3—Case study 1 pressure history during bleed down, shut-in, and lubrication operations performed on the annulus. Four buildups were measured during shut in periods. Not shown is the final pressure reading of 4,200 psi which was recorded at 568 hr.

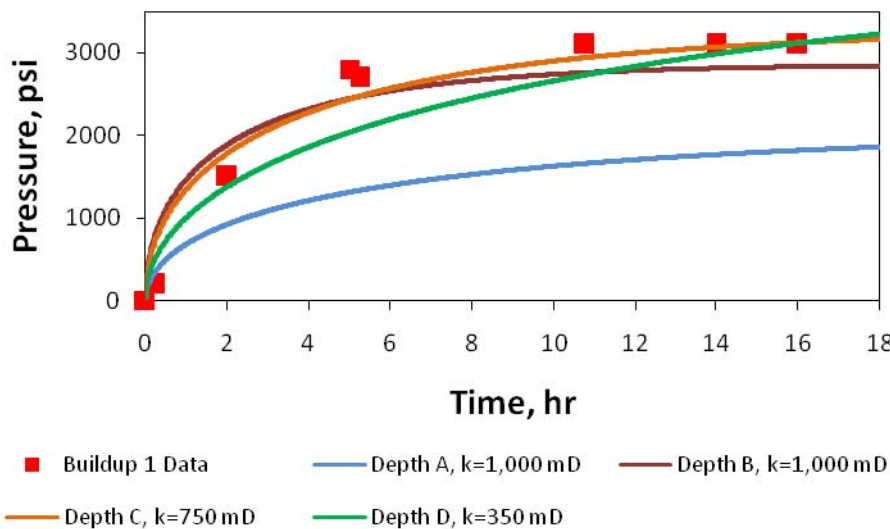


Fig. 2.4—*Buildup 1*. Leakage cannot be coming from depth A (casing seat at 10,607 ft TVD) because pressure cannot reach the recorded values. Plotted for the other depths are several different curves to illustrate the sensitivity of fits to different effective permeabilities.

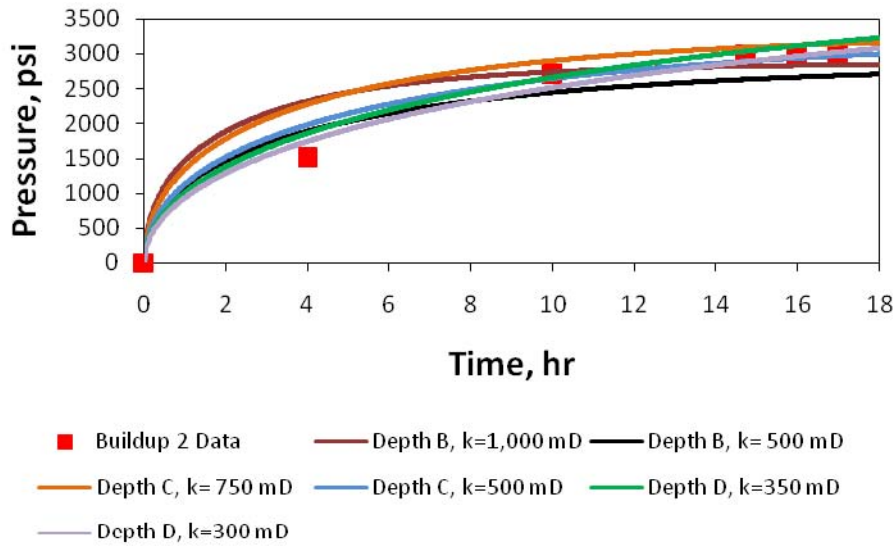


Fig. 2.5—*Buildup 2*. Curves used in buildup 1 do not match the data for second build up interval. Leakage from depth B is also ruled out because the final pressure is too low.

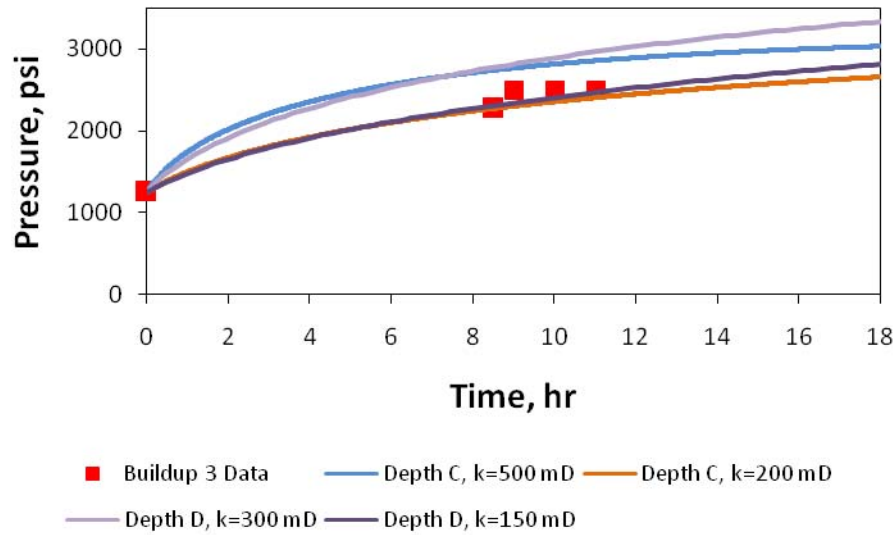


Fig. 2.6—*Buildup 3*. Previous fits do not match well here either because of the lower buildup rates. Fits from the deeper two locations are plausible when a lower permeability is used.

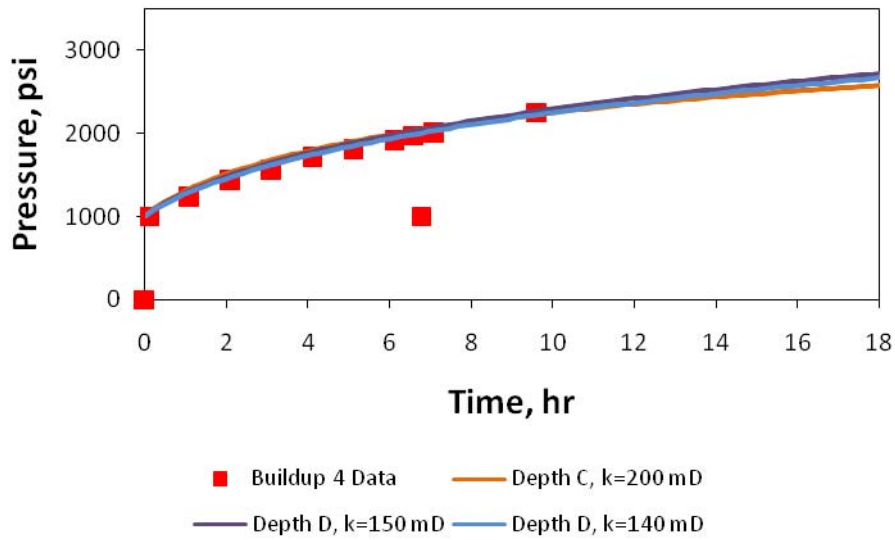


Fig. 2.7—*Buildup 4*. Previous curves (orange and purple) match well. Lack of long term pressure buildup data prevent us from identifying a leakage source depth based on these data alone.

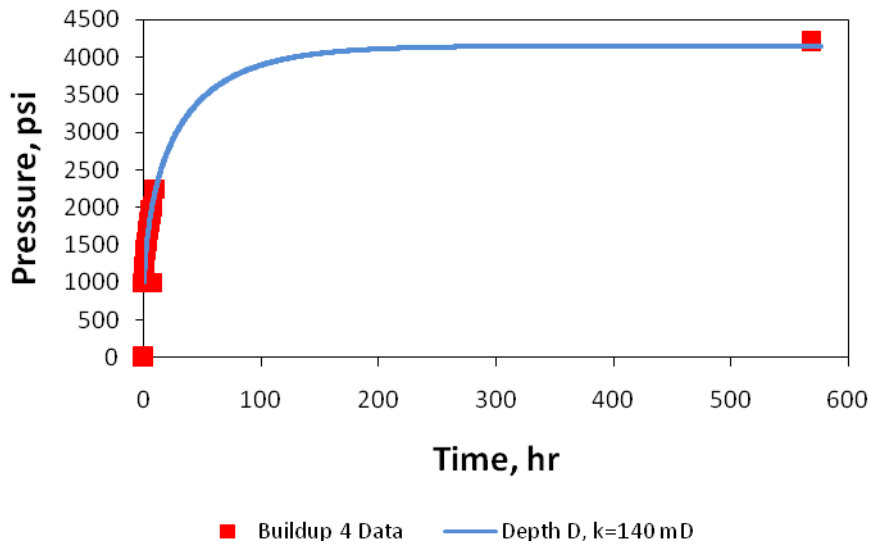


Fig. 2.8—*Buildup 4*. Best fit (Depth D, $k=140$ mD) with long time pressure measurement.

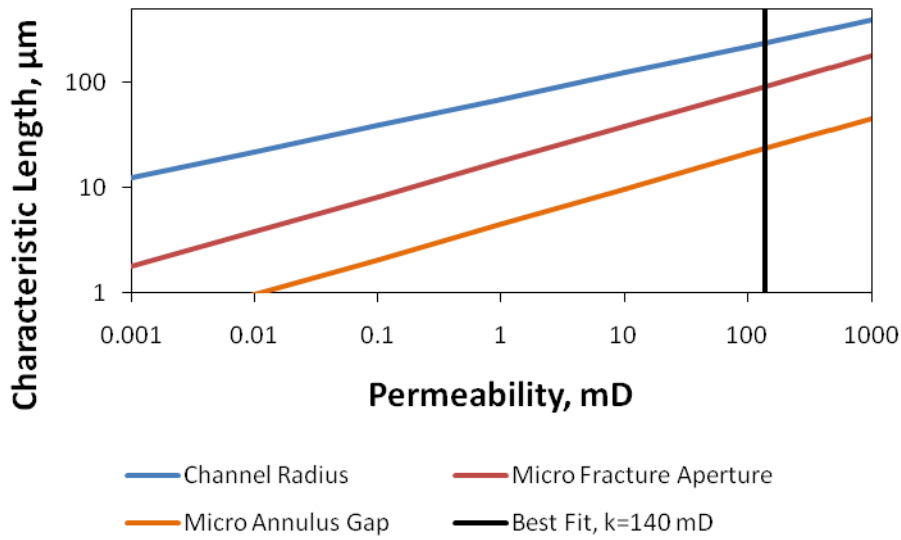


Fig. 2.9—This plot relates the best match permeability to the characteristic dimension of three equivalent geometries.

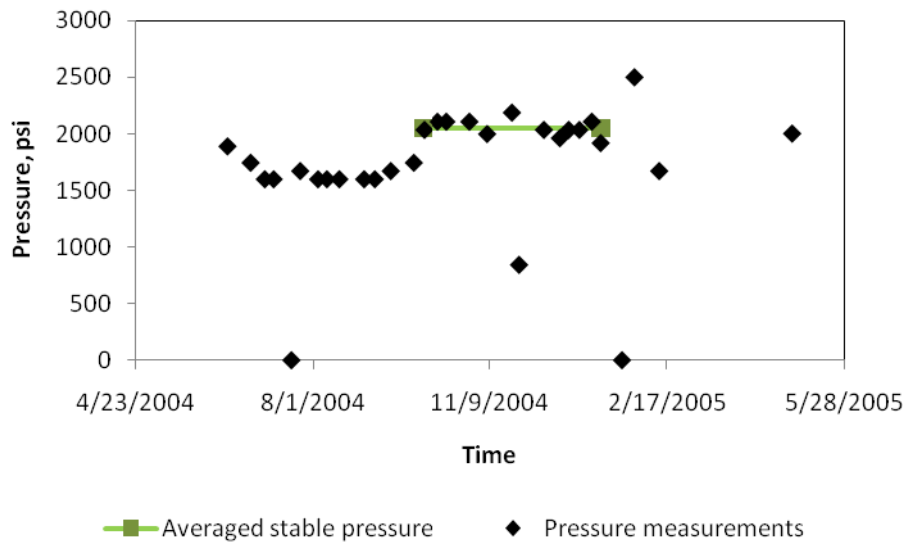


Fig. 2.10—Long term pressure measurements on the intermediate annulus in case study 2. The stabilized pressure is estimated as 2,050 psi (green line), which is the average pressure from 10/02/04 to 01/02/05, excluding the single outlier.

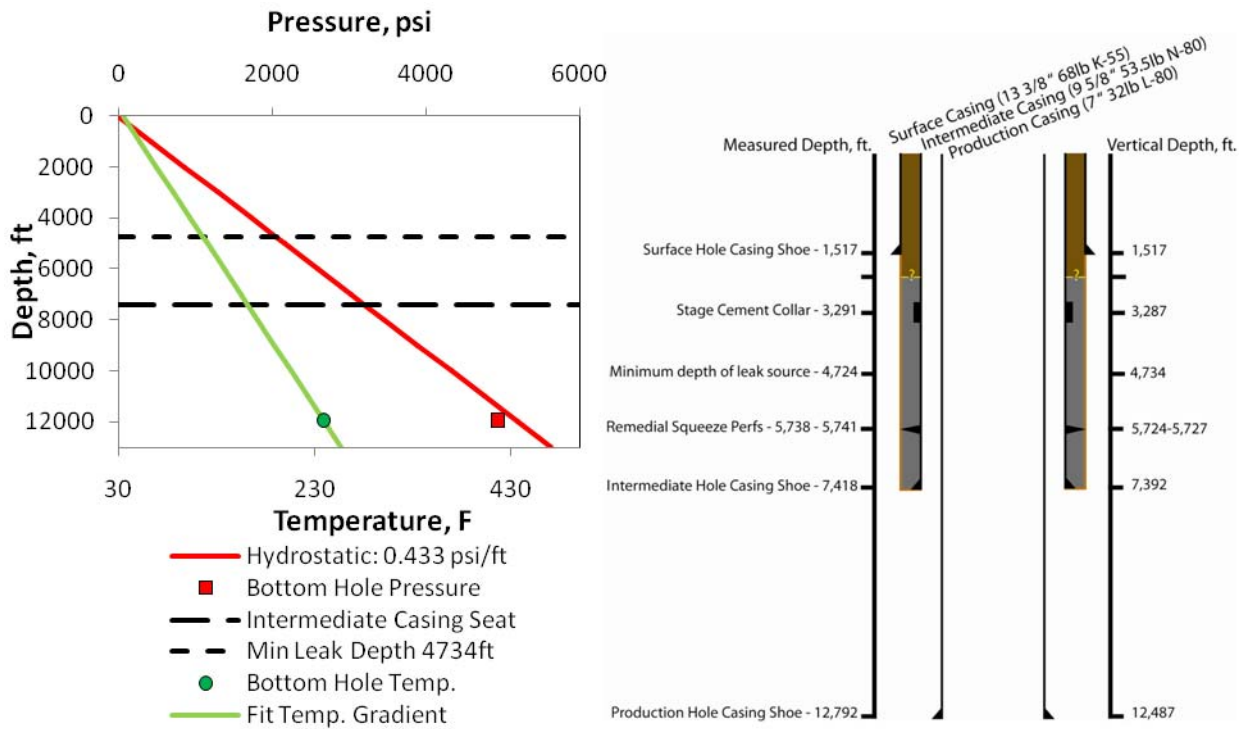


Fig. 2.11—Case study 2 wellbore schematic (right) showing relevant depths. Graph on left shows pressure and temperature gradients and interval of potential leak source.

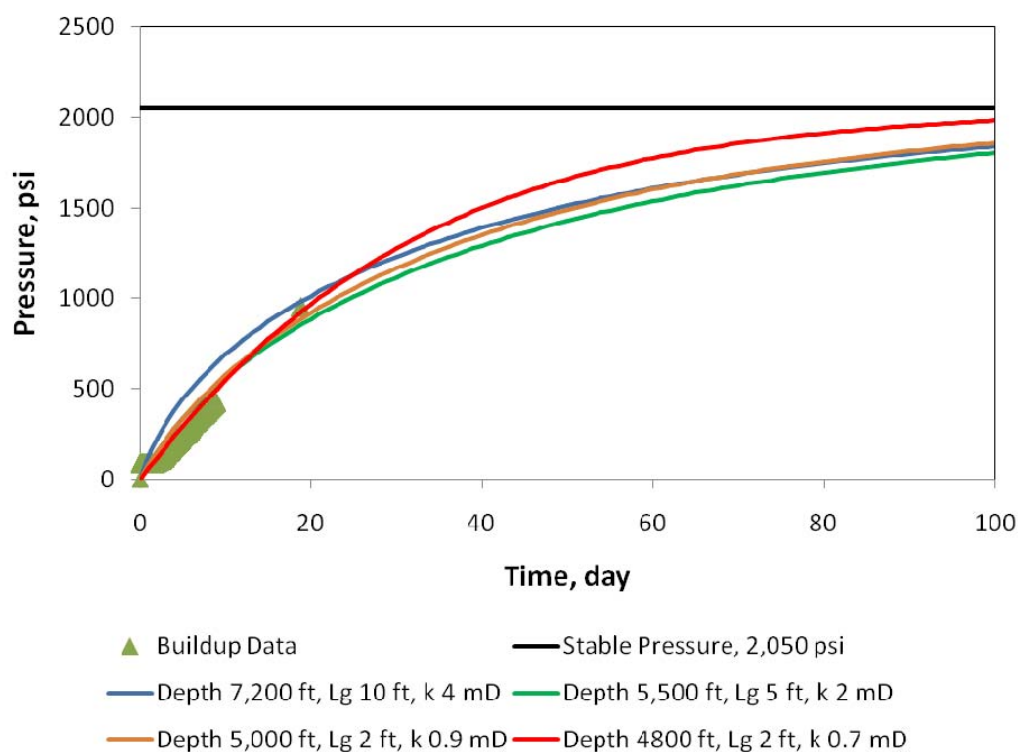


Fig. 2.12—Fitting results for four different depths for our second case study.

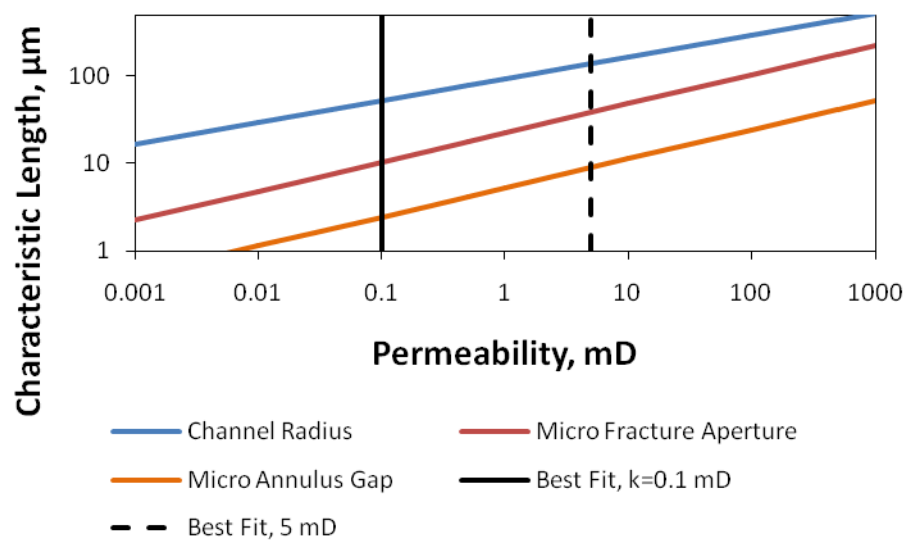


Fig. 2.13—Plotted are the equivalent geometry for the annular area and range of effective permeability determined in case study 2.

CHAPTER 3 - CEMENT CORE EXPERIMENTS WITH A CONDUCTIVE LEAKAGE PATHWAY, UNDER CONFINING STRESS AND ALTERATION OF CEMENT'S MECHANICAL PROPERTIES VIA A REACTIVE FLUID, AS AN ANALOG FOR CO₂ LEAKAGE SCENARIO

Summary

Unsuccessful zonal isolation and occurrence of sustained casing pressure indicate transport of fluids along a conductive pathway in a well's cemented annulus. Conductive pathways in cement can be grouped into three general classes: separation of the cement and formation or casing to form a micro annulus; micro fractures in the cement; and gas/mud channels in the cement matrix. In geologic storage of CO₂ similar conductive paths are most likely to be responsible for CO₂ leakage out of the reservoir along a wellbore. Moreover, cement is reactive with both CO₂ gas and acidified brine (a product of CO₂ dissolution into formation water) and the resulting cement product is of lower mechanical strength than the intact cement.

Recent research indicates that in API class H neat cement the reaction rate is slow and long term degradation of intact cement is not a risk (Kutchko *et al.*, 2008). This observation is consistent with field scale observations at a CO₂ enhanced oil recovery operation (Carey *et al.*, 2006). These results suggest that loss of well integrity from degradation of intact cement is not a significant leakage risk. Reaction at surfaces of conductive pathways raises a new set of issues, however. In any field situation a cemented annulus, and conductive pathways within it, support the effective stress of surrounding rock and pore fluid. If the mechanical properties of the opposing faces of the conductive pathway are altered by chemical reaction, or if the effective stress changes, then relative displacement (opening or closing) of the faces will occur.

Our lab has developed a system to i) create a fracture in a cement core that is representative of what one would expect in a conductive pathway within a cemented annulus and ii) measure the hydraulic conductivity of the fracture under confining stress. We use this apparatus to characterize how increasing the confining stress controls the size of the aperture. We reacted the surfaces of the fractured cores and repeated the stress/aperture measurements. The results are consistent with the points of contacts between the core halves becoming mechanically weaker after reaction.

Our observations support the possibility that conductive pathways can be self-sealing. Degradation of the cement's mechanical properties by reaction with acidic aqueous phase at the surface of the fracture would lead to a narrower pathway and thus reduced leakage rate, if effective stress is unchanged. Our ultimate goal is to project the core scale relationship onto the well scale to determine the conditions (earth stresses, cement exposure to reactive fluids, and leak source pressure) under which a conduit tends to seal.

Introduction

Ensuring sequestered carbon dioxide remains in its intended reservoir is important for both financial and safety reasons. If CO₂ makes its way back to the atmosphere, then any economic credit associated with the storage of the carbon dioxide is lost. Shallow overlying aquifers used for municipal water supply could be contaminated by escaped CO₂, as could hydrocarbon reservoirs or mineral resources. The situation is analogous to the oilfield problem of hydrocarbons moving “behind pipe”. If hydrocarbons escape from the reservoir, then the operator loses a valuable asset, and the hydrocarbons may create a hazard elsewhere in the subsurface.

Faults and wells provide the most likely path for buoyant fluids to migrate into overlying formations or reach the surface. Wells are of particular concern because they are created from the surface downward, whereas a fault might attenuate in the subsurface. The primary concern in the well is the cement's ability to successfully fulfill one of its main purposes, that of zonal isolation (Mueller *et al.*, 2004). Throughout its life, a well suffers from many phenomena that may cause loss of zonal isolation (Nelson and Guillot, 2006). These include changes in the surrounding earth stresses (e.g. pore pressure variation in adjacent rocks and changes in tectonics due to production of reservoir) and expansion and contraction of pipe as pressure and temperature within the pipe change (e.g. pressure testing, fracture jobs, water flooding, and other EOR methods). Additionally, in CO₂ sequestration operations not only will the well be under a state of stress due to ambient reservoir conditions but there will be pore pressure variations during and after injection operations and as the plume migrates within the storage volume.

The mechanisms and length scale for onset of leaks have been discussed in several papers (Reddy *et al.*, 2007; Nelson and Guillot, 2006; Mueller *et al.*, 2004). While the mechanisms and onset of leaks are highly variable, the mode of fluid transmittance is most probably flow in a micro annulus, in microfractures, or through channels in the cement. A micro-annulus is caused by casing/cement or cement/formation debonding. Microfractures are associated with tensile failure of cement. Channels in the cement occur when mud is not completely removed before cement placement or when gas enters the cement before it sets. Flow through a matrix of highly permeable cement seems to be the least frequent mode of transmittance, and is rarely discussed in the literature.

Leakage fluxes have been estimated for a population of leaky wells with a distribution of effective permeabilities (Nordbotten *et al.*, 2005). These studies assume

the permeability of a leaky well to be invariant with time. However, CO₂ sequestration, acid gas injection, and matrix stimulation all cause a reactive fluid to contact well cement. For the case of CO₂ sequestration there is the compounding fact that typical oilfield cement is chemically reactive with both free phase CO₂ gas and the acidified brine that is the product of carbon dioxide dissolution (Kutchko *et al.*, 2007; Onan, 1984; Shen and Pye, 1989). Unlike typical oilfield operations where exposure time to reactive fluids is relatively short, CO₂ and associated acidified brine might reside next to the well cement for extended periods of time (on the order of 10s to several 100s of years). The reaction rates of cement with both supercritical CO₂ and the associated acidic brine are the subject of active experimental and numerical investigation by groups in industry, academia, and the U.S. government. Their results to date show that in neat class H cement the rate of penetration of the reaction front is slow. The degradation rate when the cement is subject to supercritical CO₂ follows Fickian diffusion. When the cement is exposed to CO₂-saturated brine, the penetration rate is retarded by a diffusive barrier of carbonate that precipitates as the acid reacts (Kutchko *et al.*, 2008). Penetration rate in cement mixtures with additives such as pozzolan is still being studied, but preliminary results show no wholesale loss of cement integrity. However, reactive transport along an existing conductive pathway (microfractures etc.) remains a cause for concern on these timescales and is one of the motivations for this study.

In all wells Earth stresses exist. In the CO₂ leakage scenario the well is initially in mechanical equilibrium. When cement along an existing pathway undergoes reaction the state of equilibrium and the distribution of stress in the system are perturbed. To restore equilibrium the cement around the conduit could, because it has lower mechanical strength, deform and (partially) close the pathway. On the other hand, because of pressure from the buoyant fluid we could also see the degraded cement fail and allow propagation

of the reactive fluid to overlying, unaltered cement (Dusseault *et al.*, 2000). Thus we have a feedback loop, coupling geochemical reaction, fluid dynamics, and geomechanics. A leak path could become larger if the fluid pressure and/or cement's mechanical strength can counteract confining earth stresses, or it could become smaller as a result of the coupling.

We report here a preliminary experimental study of the coupled relationship between fluid flow in a conductive pathway; the effect confining stress has on the magnitude of the pathway aperture; the associated increase in pressure drop as fluid flows through the pathway, and finally how cement with a reacted zone forming each wall of the conductive pathway will behave when subject to variable confining stress and fluid pressure. In essence we wish to test the following hypothesis: That the altered cement will behave plastically and deform under stress so as to plug the leakage path.

Methods

SAMPLE DESCRIPTION

Samples were made using class H neat cement (density 16.5 lbm/gal; water to cement ratio: 0.388). For the sawed and epoxied cores the samples were drilled out of larger cement blocks. For the cores failed using the Brazilian method a smooth core is required so rigid thin plastic tubing (25.4 mm inner diameter) was used to hold the setting cement.

Hydrochloric acid (HCl) was used as the degrading acid on the cement (pH 0.3 or 0.5 M). Each half of the cement core was placed face down in roughly 1 mm of fluid, which was kept at a constant level by removing fluid and adding acid as needed. Additional acid was added to the system as the fluid pH began to approach basic values.

For the first acid treatment on sample D8 initially only 10 ml of solution was used. For the second acid treatment, an additional 30 ml was applied.

To create an aperture of known size with the sawed cores, a mixture of epoxy and silica flour was used to prop open the sawed faces with a bead placed along the edges. In subsequent experiments only sealant caulk was used to prevent flow outside of the fracture. The fractured cores were reassembled with a small offset (chosen by eye) in the axial direction so that the fracture was held open by asperities.

EXPERIMENT DESIGN

A. Sawed and Epoxied Cores

The objective of experiments with these cores was to verify that we could measure changes in leakage pathway geometry caused by mechanical stress. Cement cores were sawed lengthwise to create a smooth flow channel. They were reassembled to create an aperture of known size using sieved silica flour with a known maximum diameter (38 μm). The silica flour was mixed with epoxy and carefully applied along edges to prop the two halves apart. Flow experiments (using tap water) were conducted at several prescribed injection rates to verify that we could accurately determine the aperture size (see mathematical treatment section). Confining pressure was increased, then the flow experiments were repeated.

B. Brazilian Fracture Cores

The objective of experiments with these cores was to quantify the relationship between leakage pathway geometry and mechanical stress in a more realistic conductive pathway. To create a realistic fracture we used the Brazilian method to fail our cores in tension (Fig. 3.1). This method is used to indirectly determine the tensile strength of cement by applying a load on two points of a cylinder of cement (Pedam, 2007). Tensile

failure is the most likely mode of cement failure in an oil well, as cement's tensile strength is significantly lower than its compressive strength (James and Boukhelifa, 2006). Since our samples were significantly (up to 5 times) longer than typical Brazilian test samples, failure in other modes sometimes occurred. If a stress point was generated or the core was not symmetric the sample could break normal to the length of the core. Part of the sample could move from tensile failure to additional compressive failure before the remainder of the sample was failed in tension.

Some heterogeneity of the fractured sample was not an unwelcome result. Irregularities and heterogeneities tended to prevent a perfect "hand-in-glove" alignment of the two halves, leaving an aperture of a few tens of microns in average effective width. However we observed that the more intact samples, when placed in the core flood apparatus, would fit back together with even a minimal amount of confining pressure. The resulting core was nearly as impermeable as the original cement. To circumvent these problems, a small amount of caulk was placed on the core to hold pieces together during re-assembly and to hold the axial offset.

Our experimental protocol calls for inferring changes in the aperture induced by changes in confining pressure. Thus we need to characterize two confounding variables. The first is the inherent hysteresis in the system (discussed below) and the second is the initial aperture size. Regarding the second variable, we take apart the core halves after a series of pressure/aperture measurements, and then re-assemble them. We make no effort to reproduce the initial geometry because the behavior of interest is the change of aperture induced by a given change in confining stress, not the absolute value of aperture.

C. Reacted Brazilian Fracture Cores

The objective of experiments with these cores was to determine if acid/cement reaction altered the relationship confining stress and aperture size. We reacted the two

halves of a fractured core in batch mode, rather than by injecting acid through the reassembled core. This enabled us to create a significant degradation depth in a reasonable amount of time in this preliminary study. To accelerate the degradation we exposed the fracture faces to hydrochloric acid with a pH significantly lower than the expected value for CO₂-saturated brine, though significantly larger than the 10 to 30 wt. % (pH -0.5 to -1.0) HCl that was used by Nasr-El-Din *et al.* (2007). While the specific chemical reaction between HCl and cement and acidified brine and cement are not the same, the degradation of the cement's mechanical strength should be similar (see Nasr-El-Din *et al.* (2007) for HCl and Kutchko *et al.* (2007) for CO₂ reaction stoichiometry and descriptions).

The cores were fractured in the same manner as described in part B preceding. Flow tests were conducted to get a base line relationship between aperture and confining pressure. The unreacted cores were disassembled and reassembled to test repeatability of the baseline trend between confining stress and aperture. The core was disassembled again and each half placed in acid so that each fracture face was allowed to react. After some time the core was reassembled and its aperture/confining pressure relationship measured. The disassemble/react/re-assemble/flow sequence was then repeated.

EQUIPMENT

A positive displacement pump with a range of 0.01 ml/min to 9.99 ml/min fed water to the Hassler cell through a line fitted with a pressure transducer. The Hassler cell applied an axial stress mechanically, to ensure flow across the core faces, and confining pressure on the sample was applied to a rubber sleeve by hydraulic fluid. The fluid line running from the hydraulic pump to the Hassler cell had a pressure transducer affixed to measure the confining stress on the core. The outlet line was open to atmospheric pressure and timed accumulation of effluent in a 10 ml graduated cylinder was used to

measure the (nominally constant) flow rate. A National Instruments data acquisition module and software was used to record inlet pressure and confining pressure as a function of time.

FLUID FLOW THROUGH A FRACTURE

We apply classical mathematical models to determine aperture size from the flow rate and pressure drop recorded during experiments. We assume single-phase, steady state, one dimensional, horizontal flow in the experiments. Our experiments involve a cement/cement interface, and conductive pathways in cemented wellbores are commonly either tensile fractures in the cement or micro annulus debonding in the cement. We idealize both types as single slot of uniform aperture in a cylindrical core (Fig. 3.1).

Slot flow (Eq. 3.1) shows a very strong dependence of pressure drop on the aperture size (B), for a given flow rate.

$$Q = \frac{WB^3}{12} \frac{\Delta P}{\mu L} \quad (3.1)$$

where Q is the volumetric flow rate, W is the fracture width, B is the aperture size, L is the fracture length, ΔP is the pressure drop, and μ is the viscosity. This is convenient for our experiments. We anticipate relatively small changes in aperture, but these will result in a large change in pressure for a constant injection rate. Additionally, we assume that intact cement and degraded zones are impermeable since the fracture accommodates such a large amount of flow.

Eq. 3.1 also emphasizes the importance of the feedback loop studied here. For example, a 33% reduction in aperture B leads to disproportionate 70% reduction in volumetric flow rate Q ; narrowing the aperture by 67% would reduce the flow rate to less than 4% of its original value. Thus accounting for geochemical/geomechanical alterations to the aperture is important for leakage flux estimates.

CONFINING STRESS RELATION

The relation between confining stress and aperture size is complicated because the aperture is irregular. For the purposes of computing flow we idealize the fracture with a single average aperture size B , but a set of contact points between the fracture faces is responsible for holding the fracture open (Fig. 3.2). The stress acting normal to the fracture faces, σ_{zz} , is counteracted by pore fluid pressure and by compressive forces caused by deformation at the contacts as sketched in Fig. 3.2. Increasing σ_{zz} would increase the deformation at the contacts, and the two faces would move closer together by some increment ΔB . For small deformations and constant fluid pressure we may write

$$E_{eff} \frac{\Delta B}{B} = \sigma_{zz} \quad (3.2)$$

where E_{eff} is an effective Young's modulus that describes the average behavior of the asperities. In practice the range of validity of this expression, or the assumption of constant E_{eff} , is narrow. In fact, we anticipate inelastic deformation at the asperities especially when reaction has occurred. In these cases Eq. 3.2 is useful for showing the directional behavior.

Eq. 3.2 implies a coupling between geomechanics (effective stress σ_{zz} , cement mechanical properties E_{eff}) and flow (aperture B and hence the effective permeability of the conduit, Eq. 3.1). This is a key part of the feedback loop of interest in this application. Eq. 3.2 also indicates the role of the coupling between geochemistry (acid/cement reaction) and geomechanics: if the reaction reduces the mechanical strength, we expect E_{eff} to become smaller. This means a larger deformation $\Delta B/B$ would be required to support the same confining stress. Our experiments are designed to quantify this behavior.

DATA ANALYSIS

Three types of data were collected during the experiment. Confining pressure and inlet pressure were measured throughout a flow experiment. Two types of phenomena with the pressure measurements should be noted. The first two are inherent to the system. An exponential decay in confining pressure was always present; we took measurements only after waiting until the rate of decay over the flow test interval was small. Random noise and resolution limits were evident in the inlet pressure data. To minimize this error we chose appropriate pressure transducers. When a core aperture was sufficiently small and the pump rate set high, the fluid would begin to force apart the aperture. This was evident when the inlet pressure began to track with confining pressure as the latter was incremented. To get values of inlet pressure for calculating aperture size we took the average of the inlet pressure reading over the flow test time interval. Likewise to compare aperture to confining stress we took an average of the readings over the test interval. Volume of fluid collected versus time, at a given pump rate, was collected and a linear function was fit through the data using least squares. The slope of this line was the flow rate for the experiment. To minimize error a range of flow rates and resulting input pressures are measured for a given confining pressure. Plotting these values and fitting a line through the data yields a slope that is related to aperture size (Fig. 3.3). We checked the linearity of these plots for evidence of deviation from Eq. 3.1, which is possible if for example the inlet pressure is large enough to decrease the effective stress. This procedure provides us a quantitative method to characterize the relationship between confining stress and aperture size for our samples and to identify deviations in this relationship, caused by alteration of the cement by acid attack.

THEORETICAL CALCULATIONS

We performed preliminary calculations to determine appropriate pressure transducers, aperture size, and sensitivity to changes in aperture size. Fig. 3.3 highlights key system limitations identified in our study, given our equipment setup. For example if the aperture was too large, only the upper range of our pump could be used. If the aperture was too small then a small change in pump rate would yield a very large increase in pressure drop. Both extremes would add noise to the system and reduce the accuracy of our results. An aperture size of 10 μm to 50 μm was preferred for our current setup. This aperture range agrees with values estimated using sustained casing pressure analysis (Table 2.3) and similar size geometries have been presented by other researchers (Boukhelifa *et al.*, 2005).

Another important factor to consider is how a small aperture change would be resolved with the method. Fig. 3.4 illustrates how a small change ($\pm 2 \mu\text{m}$) in aperture size for three different aperture sizes would affect the flow rate/pressure drop relationship. If our core was at the upper end of the ideal aperture range, a small change in aperture would yield only a minimal change in pressure for a given flow rate. At the low end of the ideal range a very large difference in pressure drop would be observed for a given flow rate. Preliminary calculations helped us to design our experimental apparatus and create a test case core to begin experiments.

Results/Discussion

A. SAWN AND EPOXIED CORE

This set of preliminary experiments was designed to test if our experimental apparatus could successfully measure aperture size (indirectly, by means of flow rate/pressure drop measurements) and quantify small changes in aperture. A cement core

(sample B6) was sawed lengthwise, and the two halves were reassembled with the gap propped with 38 μm diameter silica flour as described previously. To induce changes in aperture we increased confining pressure on the core in steps from 200 psi to 400 psi, then 600 psi and finally 800 psi. We refer to this sequence as a “loading experiment.” After a loading experiment the confining pressure was released, but we did not measure flow rate or pressure drop during unloading.

Three loading experiments were conducted on our sample to determine hysteresis and repeatability. Results are plotted on Fig. 3.5. The first point in loading experiment 1 gives an aperture size close to the diameter of silica flour used (38 μm). For all increases in confining pressure there is a measureable decrease in aperture size. As we step through our loading experiment there seems to be a slight slope to the data. This is attributed to inelastic behavior of the epoxy/silica/cement “sandwich”. Support for this conclusion is the hysteresis: the two subsequent loading experiments on the same core show permanent deformation, with an initial aperture of 34 μm at 200 psi confining pressure, 10% less than the 37 μm in the first loading experiment. The 2nd and 3rd loading experiments show a more linear response than the first, with very similar trend of confining pressure vs. aperture size.

The key result of this experiment was its proof of the concept: this apparatus could be used to reliably infer small apertures between two impermeable half-cores, and to detect small changes in aperture as confining pressure is increased. The experiments also showed that any sealant used for re-assembling fractured cores should have minimal mechanical strength. The epoxy had as much mechanical strength as other components of the system, so its response to confining pressure complicated the relationship between confining stress and aperture size.

B. BRAZILIAN FRACTURE CORES

The first set of experiments (D8) was conducted over a range of 200 psi, 400 psi, and 600 psi confining pressure (Fig. 3.7). Aperture was calculated at three different flow rates for 200 psi and 400 psi and one flow rate at 600 psi. Initially, the core was offset but overhang at the ends was left intact. The high confining pressure at 600 psi and inlet pressures, combined with the applied axial stress caused the core to slip back into its original geometry and effectively seal. The core was removed, resealed and the overhang sanded off (~1.5 mm). Experiment 2 in sample D8 was conducted at two confining pressures and at three flow rates within each confining pressure. The overall aperture size is larger for the reassembled core in experiment 2 by ~10 μm . Nevertheless the slopes of D8 experiment 1 (-0.040) and 2 (-0.053) are consistent, indicating similar effective moduli for the fracture.

D4 experiment was prepared with its end sanded to prevent unintended closure of its fracture. Fig. 3.7 shows that while there is a decrease in aperture when D4 core was disassembled then reassembled, the slopes are nearly the same.

Similar slopes in both D8 and D4 shows that although the alignment of the cores was not exactly the same, the mechanical behavior of the core was similar. This enables us to meet our experimental objective, which is to examine the coupling between flow properties (average aperture or effective permeability), confining stress and mechanical properties of the cement (effective Young's modulus, value in reacted vs. unreacted cement).

C. REACTED BRAZILIAN FRACTURE CORES

After exposing sample D8 to acid, Fig. 3.8, we ran experiments on the core over a large range of confining pressure and flow rate. As Fig. 3.9 shows, the initial aperture size for load experiment 3 was slightly above experiment 2 but ended at roughly the same

aperture size at ~310 psi confining pressure. The slope of this set of experiments was double the slope of the data for the unreacted cores. This confirms the cement had been altered, and that the alteration is consistent with mechanical weakening (smaller E_{eff}). This is consistent with visual observation of heavily acid-reacted cement becoming softer, even gelatinous.

After load experiment 3 the core was disassembled and the core faces reacted with additional 30 ml of 0.3 pH HCl for 24 hours. At the end of the contact time, the pH was 5.0. Upon reassembly of the core halves, it became immediately apparent that the core had suffered a decrease in aperture size. The flow measurements for load experiment 4 had to be conducted at much lower pump rate than previously. The initial aperture size (at confining pressure only 50 psi; note that previous loading experiments started at 100 psi or more) was much smaller. This is consistent with significant plastic deformation of the heavily reacted contact points at small stress. Nevertheless the core exhibited the same aperture/effective stress trend in load experiment 4 as in load experiment 3. The contribution of inlet pressure to effective stress is important in load experiment 4 because the hydraulic conductivity of the fracture is much smaller.

Conclusions

A set of experiments in cement cores (fractured in tension in the style of the Brazilian test) has provided preliminary quantification of these coupled phenomena. Brine is flowed through re-assembled fractured cores as the confining pressure is increased. We find that unreacted fractured cores exhibit a characteristic dependence of change in aperture to change in confining stress. When a fractured core is reacted moderately with low pH brine, the aperture changes about twice as much for a given change in confining stress. This is consistent with acid-induced degradation of the

mechanical strength of the cement matrix on the fracture surface. When a fracture core is reacted extensively with low pH brine, substantial plastic deformation occurs as the core is brought to the initial (smallest) value of confining stress.

These results provide qualitative support for the possibility that “leaky wells” may be self-sealing against fluxes of CO₂ rich fluids. This hypothesis warranted further investigation, with emphasis on more detailed control of loading cycles and exposure conditions.

Table 3.1—D8 results from core flooding

Data run	Average confining pressure, psi	Average flow rate, ml/s	Average inlet pressure, psi	Inferred aperture, μm
1	210.5	0.047	11.47	33.8
	207.6	0.015	5.63	29.3
	206.2	0.080	22.78	32.1
	407.3	0.016	12.30	23.0
	412.5	0.048	39.01	22.6
	414.3	0.082	77.40	21.5
	598.8	0.016	29.13	17.3
2	208.7	0.031	4.31	40.7
	208.1	0.065	7.48	43.4
	208.0	0.082	8.80	44.4
	301.5	0.033	5.82	37.6
	300.1	0.066	10.92	38.4
	299.9	0.088	14.43	38.6
3	124.9	0.015	1.09	50.6
	122.4	0.033	1.56	58.3
	122.4	0.067	2.56	62.7
	161.5	0.017	1.20	51.0
	160.7	0.033	1.97	54.0
	160.7	0.066	3.50	56.2
	202.2	0.017	1.67	45.7
	201.9	0.033	2.77	48.2
	202.1	0.064	4.61	50.7
	263.6	0.016	2.16	41.1
	263.1	0.033	3.65	44.0
	263.0	0.034	3.75	44.0
	313.0	0.008	2.11	32.9
	314.1	0.018	3.46	36.6
315.2	0.062	8.46	41.0	
4	87.2	0.001	7.33	10.5
	86.0	0.001	8.44	10.0
	85.9	0.013	16.67	19.4
	86.0	0.015	22.59	18.4
	154.6	0.008	62.90	10.6
	155.1	0.009	85.85	10.0
	144.8	0.001	16.96	8.2
	205.7	0.001	41.41	6.1
	164.9	0.001	45.12	5.9

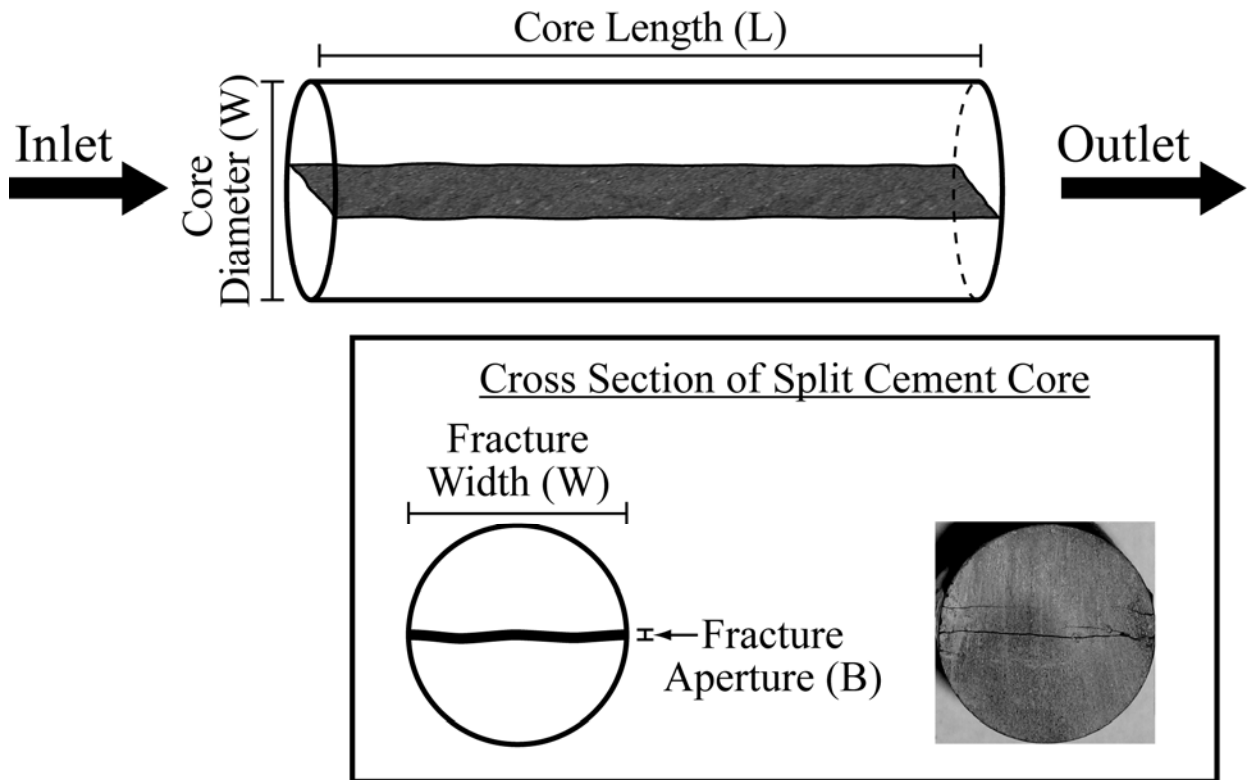


Fig. 3.1 – Schematic diagram of cores with a conductive pathway and key geometries labeled. Image is of actual cement sample with conductive pathway caused by tensile failure.

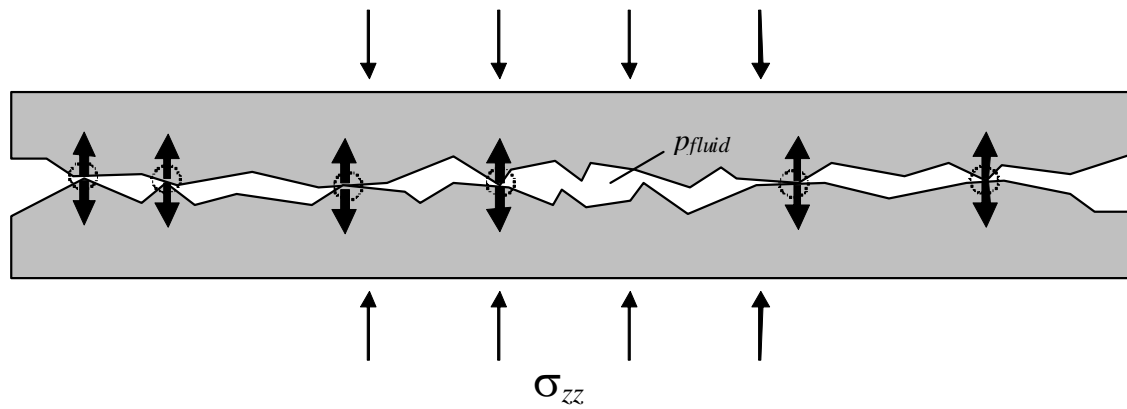


Fig. 3.2 – The effective stress on a fracture causes deformation of the material at the asperities holding the fracture open. Increasing the effective stress reduces the average aperture of the fracture.

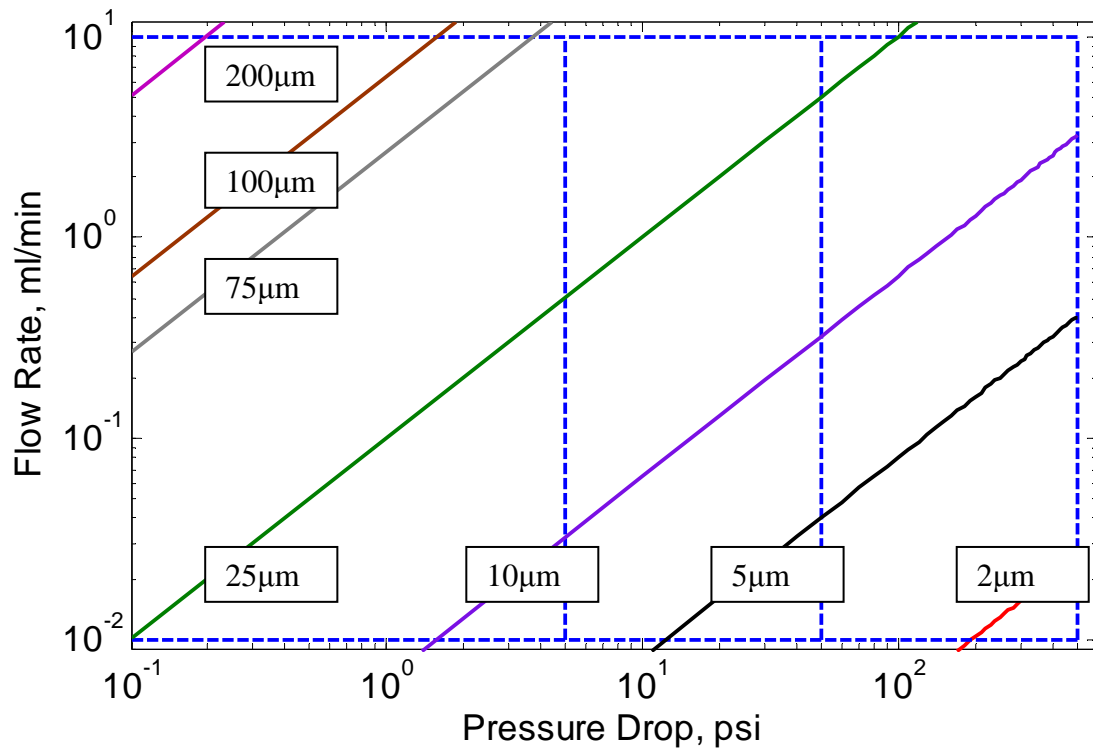


Fig. 3.3 – Pressure drop vs. pump volumetric flow rates for different aperture sizes. The blue vertical dashed lines represent upper limits for our pressure transducers (50 psi, 100 psi, and 500 psi). The horizontal blue lines represent our pump's flow rate range (0.01 ml/min to 9.99 ml/min).

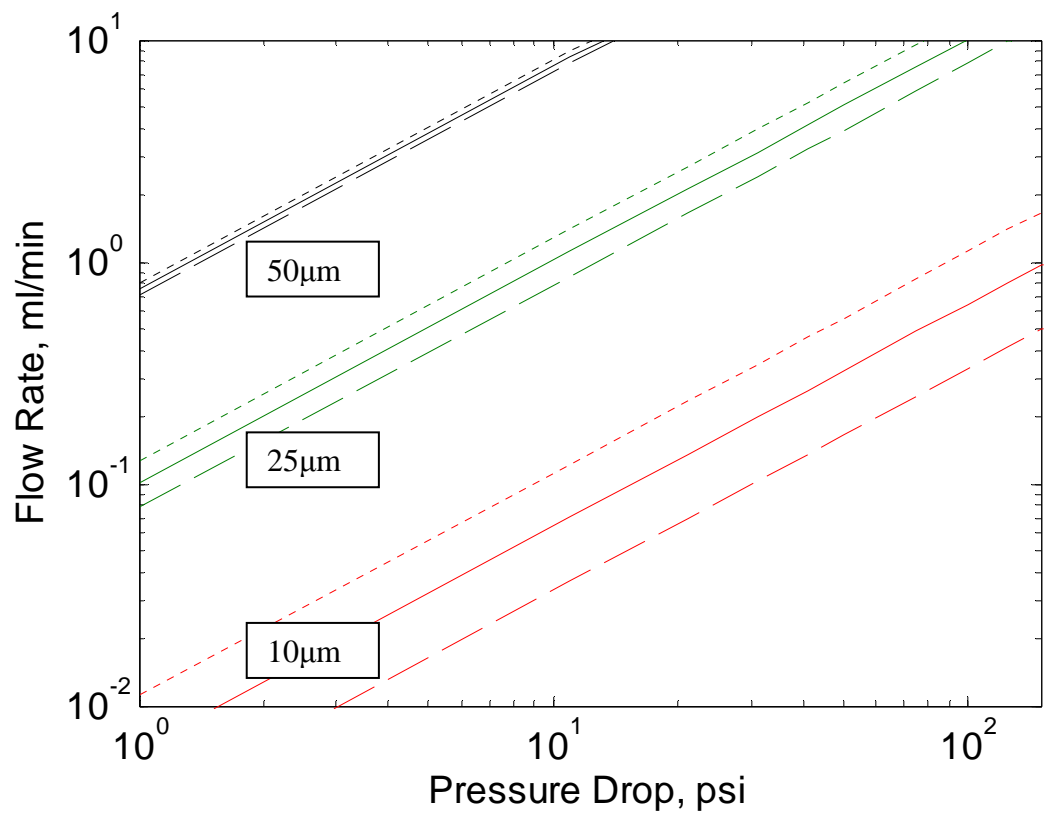



Fig. 3.4 – How a small change in aperture size can be resolved with our current equipment setup. Solid lines are for indicated aperture size; dotted lines show effect of reducing aperture by $2\mu\text{m}$ and dashed lines are for increasing aperture by $2\mu\text{m}$.

Cement core sawn and resealed with 38 μ m silica flour and epoxy running down the edges

Confining Pressure Range	psi
Red Line	200
Green Line	400
Blue Line	600
Black Line	800

 : Indicates aperture decrease

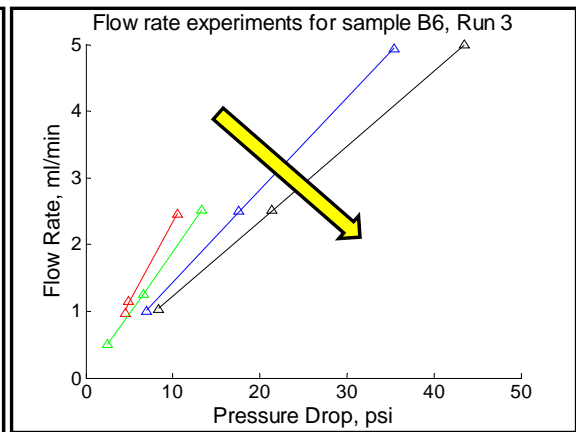
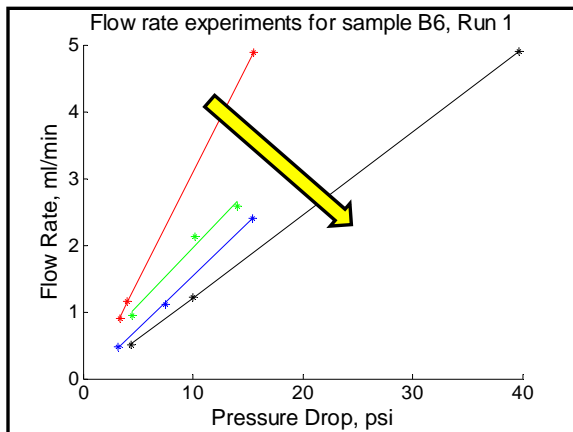
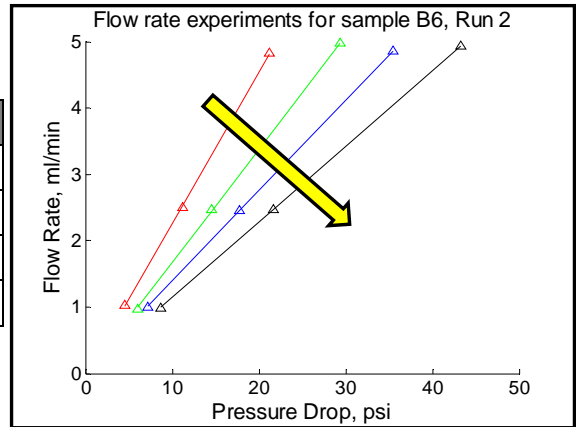


Fig. 3.5 – Three loading experiments for sawed and epoxied core at several flow rates (points within colored line) over a range of confining pressure. Each line represents a fixed confining pressure and its slope is related to the effective aperture of the fracture. In all experiments as confining pressure increases, the aperture size is decreased (yellow arrow).

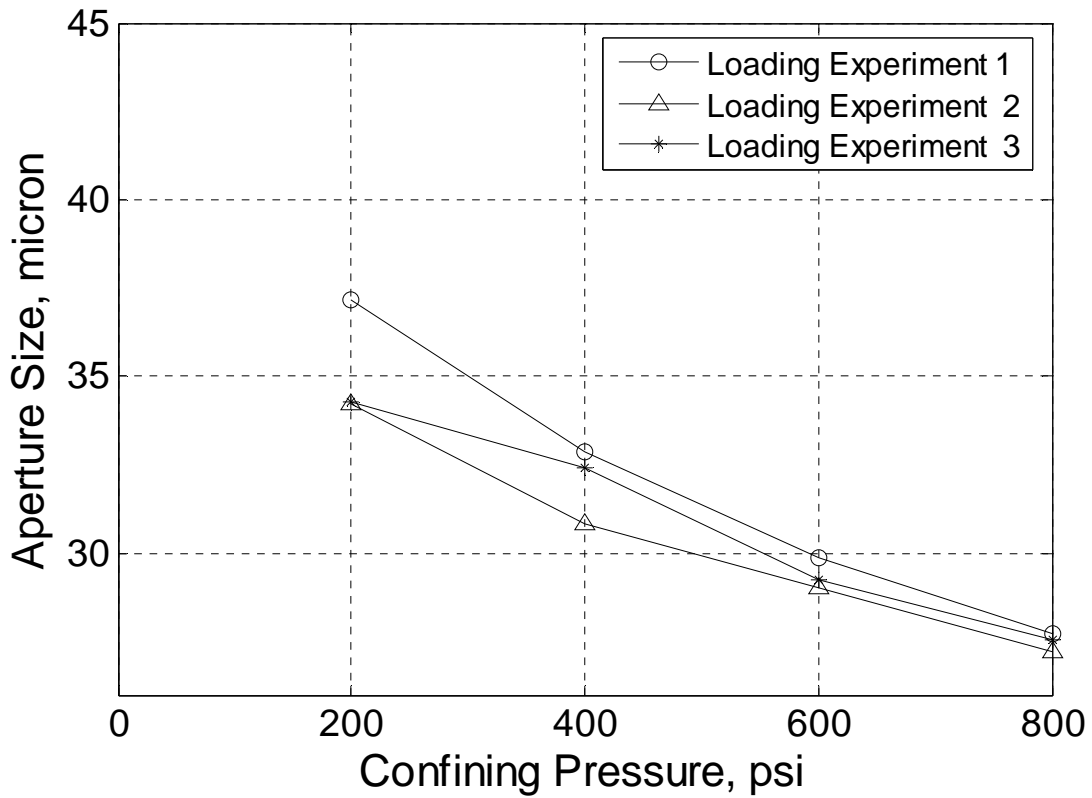


Fig. 3.6 – Relation between aperture size and confining pressure for different incremental load experiments on sample B6.

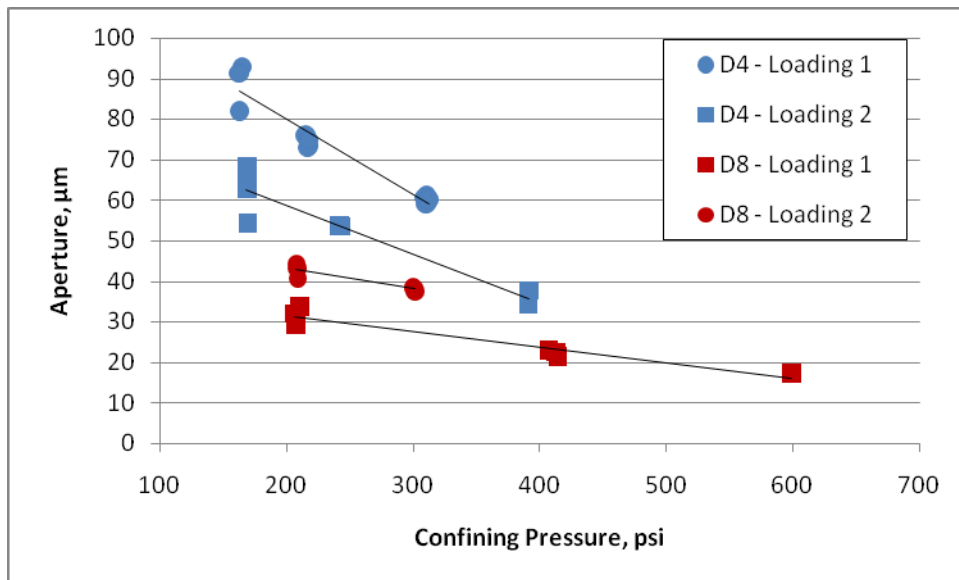


Fig. 3.7 – Unreacted fractured cement cores show a characteristic decrease in aperture size as confining stress increases. The inlet pressure during the flow experiments is small, so the effective stress is approximately equal to the confining stress.

Sample D8 before reaction



Sample D8 after reaction



*Core is 14.0 cm in length

Fig. 3.8 – Before and after images of sample D8, which was subject to reaction with HCl.

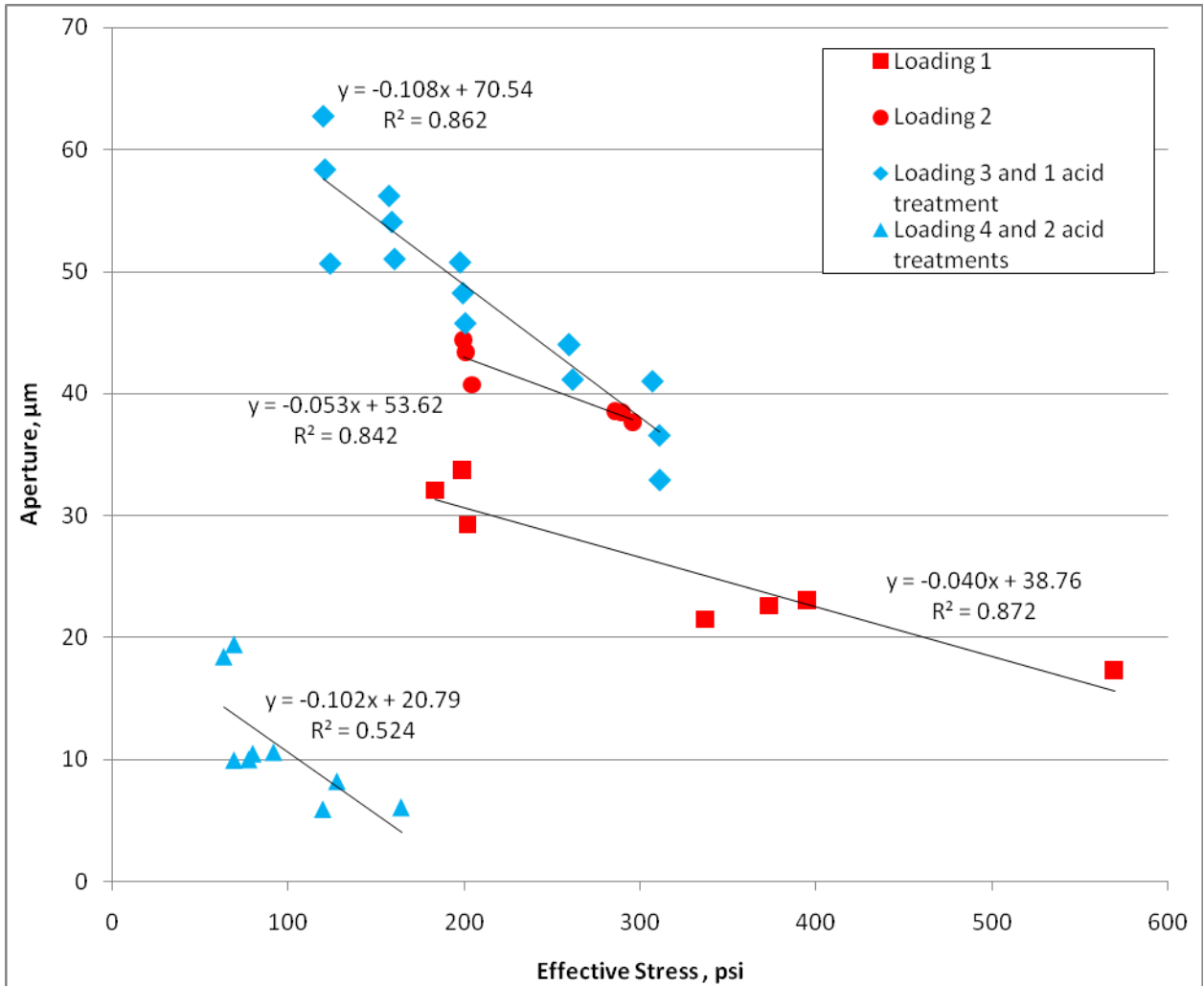


Fig. 3.9 – Fractured cement cores reacted with acid (blue points) exhibit steeper trends of aperture vs. effective stress than unreacted cores (red points). The heavily reacted sample (blue triangles, Load Experiment 4) undergoes significant plastic deformation as the core is brought to the initial confining pressure of 50 psi. The acid reaction reduces the mechanical strength of the cement, allowing faster closure as confining stress increases.

CHAPTER 4 - THE INFLUENCE OF CONFINING STRESS AND CHEMICAL ALTERATION ON CONDUCTIVE PATHWAYS WITHIN WELLBORE CEMENT

Summary

Following on proof of concept experiments presented in chapter 3 we conduct more controlled experiments to study the coupled system discussed previously. These new experiments measure flow through a fracture in a core, from which we infer its effective aperture as a function of confining pressure with more resolution. Class H neat cement was cast in cylindrical cores and fractured using the Brazilian method to create a realistic fracture. Core halves were reassembled with a small offset to prevent mating, and then sealed to ensure flow only through the fracture. We observe a systematic variation in effective aperture, and hence in conductivity, with confining stress. The variation is consistent with behavior reported in the literature (Witherspoon *et al.*, 1980). The disassembled fracture faces were then degraded with hydrochloric acid to simulate exposure to CO₂-saturated brine along this conductive pathway. A reassembled, lightly reacted fracture behaves similarly to the unreacted fracture. A heavily reacted fracture closes much faster as confining stress increases. Thus the coupling between reaction and geomechanics in the field will strongly affect the leakage rate; indeed, it raises the possibility that leaks could be self-sealing.

Fracture Flow Experiments

BACKGROUND/THEORY

We continue to focus on one of the most likely conductive pathways in the casing/cement/earth system, a single fracture created by tensile failure. Our experiment technique and analysis was much improved after discovering work by Paul Witherspoon

and others conducted at Lawrence Berkeley National Labs in the late 70s and early 80s. Their work showed that fracture flow can be modeled using the cubic law for flow between parallel plates (Witherspoon *et al.*, 1980). The fracture aperture strongly depends on any applied confining pressure (Tsang and Witherspoon, 1981 and Tsang and Witherspoon, 1983). Using loading cycles while flowing fluid through the fracture Tsang *et al.* were able to show that increasing the confining pressure on the sample decreased the aperture size in a straightforward relationship. Though loading cycles showed hysteresis and permanent deformation, with repeated loading the relationship became more reproducible. Tsang *et al.* attribute this to strain hardening, as the taller and thinner asperities on the fracture surface are broken and the shorter, broader asperities are able to accommodate the confining stress.

The relationship between aperture size and confining stress is a function of several parameters: the morphology of the fracture surfaces (asperity heights and distribution), the loading history of the fracture, and the mechanical strength of the material. If, in an appropriately strain hardened sample, the mechanical strength of the fracture surfaces were to be altered, the loading cycle would have a significantly different shape. We design our experiments to exploit this relationship.

Our preliminary study (Huerta *et al.*, 2008 and Ch. 3 of this thesis) showed that using a Hassler cell apparatus we could accurately infer an effective fracture aperture and characterize the relationship between changes in aperture size with change in confining stress during pressure cycles. We also found evidence that altering the fracture face of a cement core could have an effect on the aperture size to confining stress relationship for our samples. Our present study is an expansion of those findings.

METHODS

Equipment and Sample Description

The core flow equipment consisted of a Hassler core flow cell (Fig. 4.1 – Top Right) which can accommodate cores one inch in diameter and one foot in length. We use two pressure transducers, one to measure the inlet fluid pressure and the other to measure confining pressure on the core. Pressure data was digitally recorded using National Instruments data acquisition software. To push the water through the core a constant flow positive displacement pump was used (Fig. 4.1 – Top Left), with flow rate between 0.01 ml/min and 10.0 ml/min. Flow rate was measured by recording fluid volume collected during the experiment.

Samples were created from neat class H cement. We cured the cement at 125°F and atmospheric pressure. To create the conductive pathway we used the Brazilian method to create a tension fracture along the length of the core. To prevent the possibility of the core faces from mating when re-assembled, and to ensure a conductive pathway of some significant initial aperture size we offset the cores lengthwise by a small amount (1 mm to 2 mm) and shaved down the overlapping end sections of the core. To prevent fluid from flowing around the outside of the fracture we applied caulk with negligible mechanical strength to the outside of the core, along the fracture.

For the acid exposure we separated the core halves and placed them face down in a Pyrex dish (Fig. 4.1 – Bottom Right). The halves rested on glass stands, which made a few point contacts with the fracture face. This ensured that essentially all the fracture face was exposed to the acidic fluid (Fig. 4.1 – Bottom Left). This assembly was placed on a stir plate to ensure a well-mixed fluid as the reaction proceeded. Acidity of the fluid was monitored with time using a pH probe.

Experiment Procedure and Data Analysis

The key to all analysis in this study is the relationship between effective aperture and confining pressure (or, in a few cases, the effective confining pressure, which is the difference between confining pressure and fluid pressure within the fracture.) To obtain this relationship, a fractured core was placed in the Hassler cell with a prescribed confining pressure. The injection pump was turned on and once steady state was achieved we performed a **test**, which consisted of recording the confining pressure, inlet pressure, and time to collect a predetermined volume of fluid. Two more tests were conducted at the same confining pressure, each with a higher flow rate (and correspondingly higher inlet pressure). These three tests are termed an **experiment**, which is used to calculate the effective aperture size at the given confining pressure. The confining pressure was then changed and more experiments performed. To determine the aperture-confining stress relationship we performed a **cycle**, in which the confining pressure was incremented several times. Experiments were conducted at each value of confining pressure. This loading portion of the cycle continued until we reached a maximum confining pressure (usually 750 psia). The unloading portion of the cycle consisted of decreasing the confining pressure and conducting experiments at various points along the unload path. We repeated cycles to test for strain-hardening or other alteration of the mechanical strength of the fracture faces.

Flow rate was determined by taking a least squares fit between the volume of fluid collected and the experiment time. The mean inlet pressure during an experiment was used. To determine the effective aperture size at a given confining stress we fit a straight line through the flow rate (Q) versus pressure drop (ΔP) data (Fig. 4.2). The slope (m) is proportional to the cube of the aperture size (B). In Fig. 4.2 the red arrow indicates how confining stress changes the slope of ($Q/\Delta P$): as confining pressure increases, the

slope decreases and so does the aperture size. This is best shown in the right hand plot of Fig. 4.2, which is a full loading/unloading cycle on a cement core. The colored data points correspond to the colored lines in the left panel and show the decrease in aperture as confining pressure increases.

The acid exposure portion of the experiment consisted of placing the core faces in hydrochloric acid adjusted to a pH of 3.5. Once reaction increased the pH of the fluid above 7 the liquid was removed using a pipette and fresh acid was placed in the container. This was repeated frequently; the total moles of acid reacted with the cement was recorded for each experiment.

Experiment Plan

Table 4.1 summarizes the experimental procedure. Each core undergoes a **baseline** experiment which consisted of three full loading cycles. Aperture measurements were conducted at three or four pressures along the loading path and at three or four pressures along the unloading path. One aperture measurement was made at the peak confining stress. The purpose of the multiple cycles was to characterize the initial (unreacted) relationship between aperture and confining stress and to strain harden the sample. The core was then taken out of the Hassler cell, taken apart and then resealed. Two additional cycles were conducted on the reassembled core. The purpose of these cycles was to determine whether the new alignment of the fracture faces that is inevitable when the core halves are re-assembled changed the relationship between aperture and confining pressure. This check is necessary because the acidization procedure required disassembly of the core. After the second set of cycles the core was removed and **placed in the acid** for a set period. After removal from the acid, the core halves were re-assembled and sealed and a set of **acid study** cycles were performed on the sample. After the baseline/acid treatment/acid study, each core was treated differently and will be

discussed in the respective results section. We present results from two cement cores (Table 4.2).

Results/Discussion

SAMPLE 1 (BB8)

For our first sample we used flow rates (ml/min) of 1.0, 1.5, and 2.0. Corresponding inlet pressures ranged from a few psi to near 200 psi. At the latter values the effective confining pressure is substantially smaller than the confining pressure; we note this effect when relevant. Confining pressure measurements (psi) were taken at 200, 300, 500, and 700 for the loading cycles; 800 at peak confining, and 700, 500, 300, and 200 during the unloading portion of the cycle. Fig. 4.3 (Top Left) shows the baseline results for sample BB8. Cycle 1 aperture size begins at 26 μm and drops to 16 μm at peak load; the aperture is 19 μm for the smallest measured unloading pressure. In Cycle 2 the aperture starts around 22 μm . The value differs from the aperture at the end of Cycle 1 because the confining pressure is reduced to zero at the end of each cycle. This permits some re-arrangement of the fracture faces when re-loading occurs on the next cycle. In Cycle 2 the aperture decreases to 15 μm as the confining pressure increases. It opens back up to at least 20 μm during unloading. In Cycle 3 the aperture begins around 21 μm and ends at 12 μm during loading, then unloads to a value of 16 μm . At the end of Cycle 3 the core was taken apart, resealed with caulk and retested. The initial aperture for Cycle 4 was larger than Cycle 1, at 33 μm (due to reseating of fracture asperities). It quickly dropped to 14 μm at maximum loading, returning to 20 μm during unloading. The final Cycle (5) follows Cycle 3 quite well, starting at 22 μm and reaching 13 μm at maximum confining stress. It unloaded to at least 18 μm .

The baseline results for this sample follow the expected relationship between confining stress and aperture size quite well (Iwai, 1976). As the sample repeatedly cycled, asperities crush and the fracture becomes “strain hardened” – moving from cycles with permanent deformation, to approximately elastic (reversible paths) behavior. Hysteresis during loading and unloading cycles is also evident. Even when the sample is taken apart and resealed the core quickly approaches the previous strain hardened behavior. Initial variability of aperture is inevitable any time the core is disassembled then reassembled. For our purposes the important observation is that the core still exhibits the strain-hardened behavior obtained in the previous cycles.

After acid treatment conditions shown in Table 4.2, sample BB8 (Fig. 4.4 – Right) was retested for three cycles. Fig. 4.3 (Top Left) shows the results from the cycle test. The flow rate range was dropped from the base line to 1.0, 1.5, and 2.0 ml/min to keep inlet pressure (ranging from a few psi to hundreds of psi, depending on confining pressure) below the pressure transducer limit. The baseline confining pressure schedule was followed. Initial aperture size is quite large (52 μm) but during loading it quickly drops to near the aperture size developed at maximum load (14 μm). The aperture recovered to 24 μm during unloading. In Cycle 2 the aperture starts out at 25 μm and is 13 μm at peak load, opening up to 19 μm at the lowest unloading confining pressure measured. The final Cycle (3) aperture measurements are: 20 μm at the lowest loading path confining pressure, 12 μm at peak load, and to 18 μm at lowest unload in confining pressure.

The acid treatment did not significantly alter the aperture/confining stress relationship in sample BB8 (Fig. 4.3 – Bottom Right). There are several possible reasons for the absence of an effect. The first is there was not significant reaction during the acid test. Secondly, confining pressure range used with sample BB8 might affect the results.

In our previous work (Huerta *et al.*, 2008); we used a lower peak load. Increased load results in more asperity deformation during strain hardening and overall smoother fracture faces. The remaining asperities are shorter, broader, and able to withstand more loading. A combination of both factors is also possible since during acid treatment the reactive fluid must penetrate into broader asperities to significantly alter the mechanical strength of the fracture.

Sample 2 (F14B)

For baseline results a pump rate (ml/min) of 2.0, 3.0, and 4.0 was used and the corresponding inlet pressure was in the range of 0.5 psi to 3 psi, depending on the confining pressure and cycle number. The low inlet pressure induced significant uncertainty into aperture size calculation. Fig. 4.5 shows the aperture/confining pressure trends for baseline and after exposure to acid cycles. Aperture starts out around 115 μm and decreases to around 90 μm during the first load cycle. During the second load cycle aperture starts out around 83 μm and decreases to 52 μm at maximum loading (550 psi). Cycle 3 starts out at 83 μm and decreases to about 67 μm . The sample was then taken apart and resealed. The initial aperture size for Cycle 4 is 99 μm and drops to 76 μm at maximum loading. Cycle 5 starts at around 84 μm and drops to around 62 μm . During the unloading cycle significant hysteresis is evident. The non-monotonic behavior is attributed to noise in the inlet pressure signal (the absolute pressures are small for large apertures). The trend of aperture vs. confining pressure is consistent with earlier results (Huerta *et al.*, 2008) and behaves according to model expectations (Iwai, 1976). Aperture size is never below 50 μm and 60 μm seems to be about the point where the core begins to behave elastically, when the maximum load is at 550 psi confining.

After the baseline cycles, the core (Fig. 4.4) was acid treated as shown in Table 4.2. About five times as much acid was consumed in this treatment as in the previous

core. We thus anticipate more effect on the aperture/confining pressure relationship. A single loading cycle was performed using 1, 2, and 3.5 ml/min flow rate. The green line in Fig. 4.5 shows the results of this partial cycle. The first three measurements (red circle) were conducted at the same confining stress but on different days. A significant drop in aperture occurred between these experiments, though they were conducted at the same nominal confining pressure. We attribute this to the fact that the confining pressure was raised 10 psi over the desired values. Over pressurizing the core is necessary because some confining pressure becomes attenuated by system compressibility and minor fluid loss during the experiment. This observation suggests the core's mechanical strength was significantly altered during acid treatment, so that plastic deformation occurs much more readily. The aperture size also decreases more at a lower confining pressure, compared to its behavior during the baseline cycles. Aperture size at 500 psi confining pressure was 10 μm . At this point, the inlet fluid pressure was approaching the pressure transducer limit so a test near the baseline maximum (550 psi) was not possible. Likewise, equipment limitations prevented further experiments below 350 psi on the unloading path (green circle). The small aperture size prevented further analysis of this sample but it is clear that the cement's mechanical properties had been substantially altered by the acid attack. Consequently the fracture deformed to a much narrower aperture than the unreacted fracture. This supports the possibility that leakage pathways along a wellbore that involve cement could be self-sealing to CO_2 -rich fluids.

Conclusions

Cyclic loading of naturally fractured cement cores shows a decrease of aperture size with increased confining stress, hysteresis in loading/unloading cycle, and strain-hardening. Exposing cement fracture faces to weak acid alters the chemical and

mechanical properties of the faces. Depending on the extent of reaction, the mechanical weakening permits a much more rapid closure of aperture as confining stress increases. Degradation of cement by CO₂-rich fluids coupled with decreasing reservoir fluid pressure could render leaky wellbores self sealing.

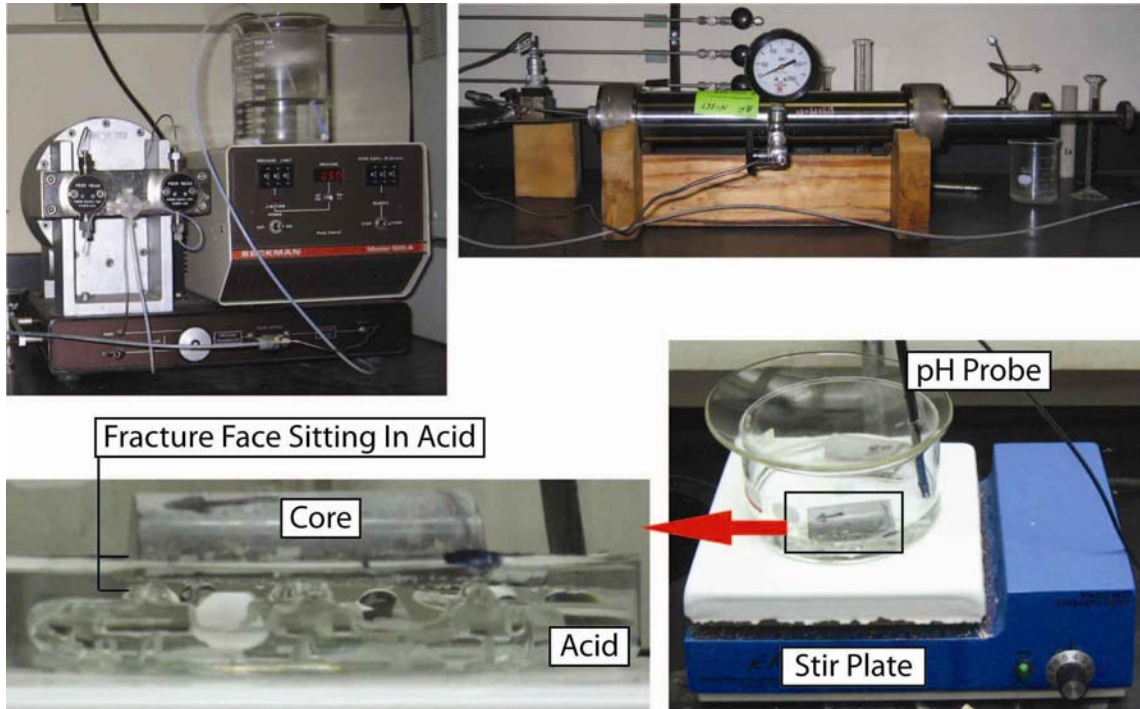


Fig. 4.1 – Equipment setup. (Top Left) Fluid pump. (Top Right) Hassler cell used to hold the cement cores for fluid flow experiments under different confining pressures. (Bottom Right) Acid reaction setup consists of a glass dish to hold the acid and cement, a pH probe, and a stir plate. (Bottom Left) Close up of one half of cement core sitting with its fracture face exposed to acidic fluid.

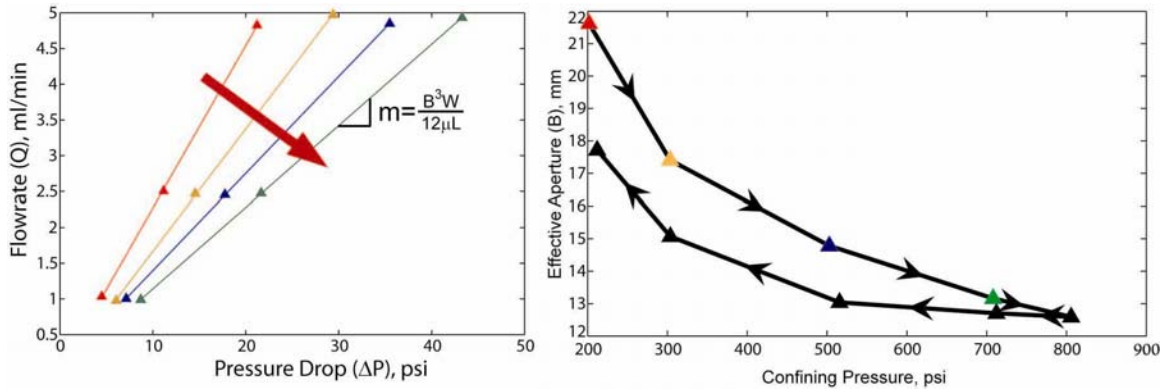


Fig. 4.2 – (Left) Four flow rate experiments (colored lines), consisting of three flow tests (triangles) for each. Each experiment was conducted at a different confining pressure during the loading part of a cycle. The red arrow illustrates the trend of effective aperture size as confining pressure increases. (Right) Colored triangles show effective aperture obtained from corresponding confining pressure experiment. The black arrows indicate the direction of loading and unloading during our cycles.

Table 4.1 - Schematic of the typical procedure used in our study

Procedure	Cycle Number
Baseline Study	1
	2
	3
	Separate and Reseal Core
	4
	5
Acid Treatment	X days
Acid Study	1
	2
	3

Single Cycle Confining Pressure Schedule, psi	
Loading	200, 300, 500, 700
Peak	800
Unloading	700, 500, 300, 200, 0

Pump Rates Used, ml/min
2.0, 3.0, 4.0

Table 4.2 - Experiment conditions for the two cores used in this study

Sample Name	Dimensions [D×L], cm	Acid Exposure [time exposed/ moles consumed]
BB8	2.6×5.15	7 days / 4.78×10^{-4}
F14B	2.5×4.9	12 days / 2.0×10^{-3}

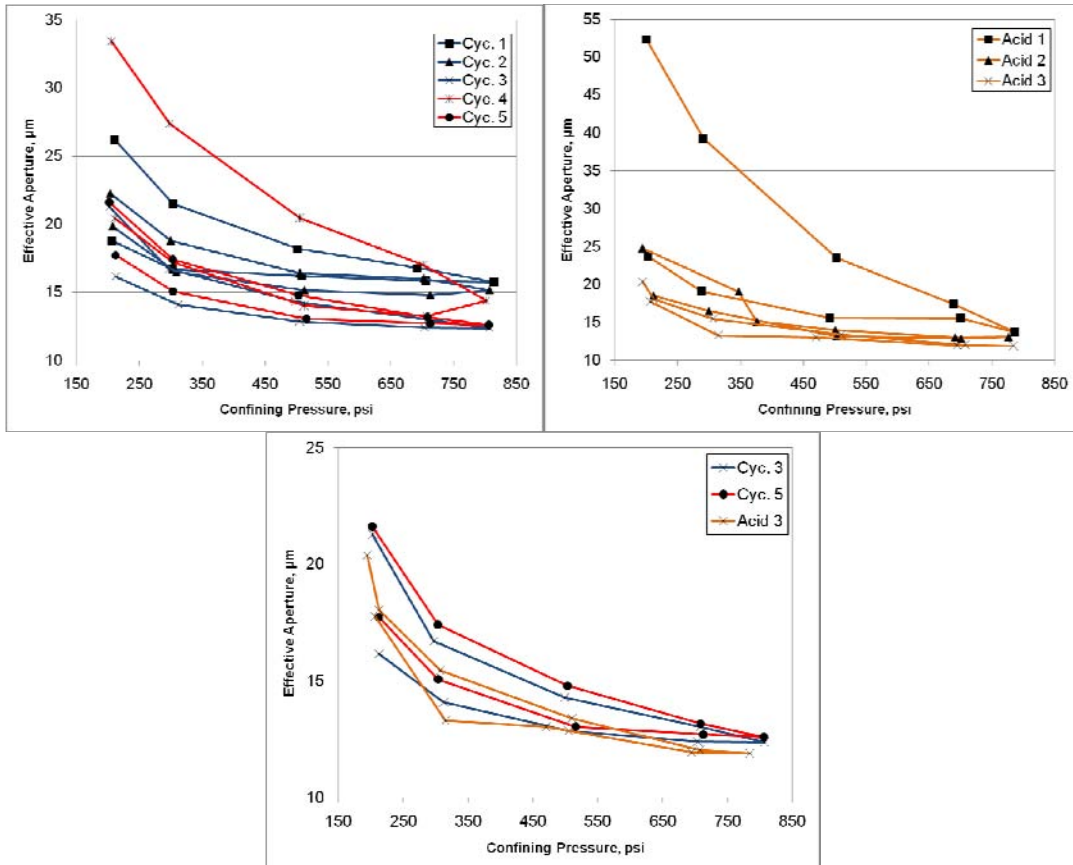


Fig. 4.3 – The top left plot shows the baseline cycles for sample BB8. The top right shows the cycles after the core has been reacted with acid once. The bottom shows the strain hardened behavior developed in the baseline study is still present after the acid exposure.

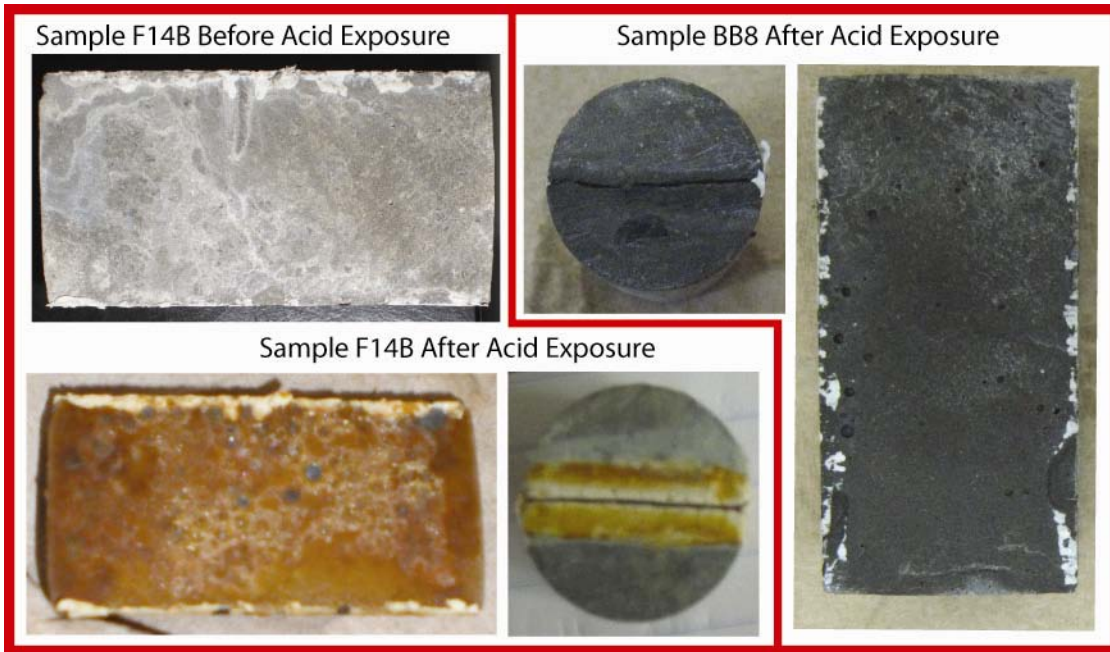


Fig. 4.4 – The three images of on the left of the dividing red line are of sample F14B. The two on the right are of sample BB8. Note the significant (orange) color alteration across the fracture face in sample F14B after acid exposure. Also note that while sample BB8 was also exposed to acid, it was significantly less altered than sample F14B.

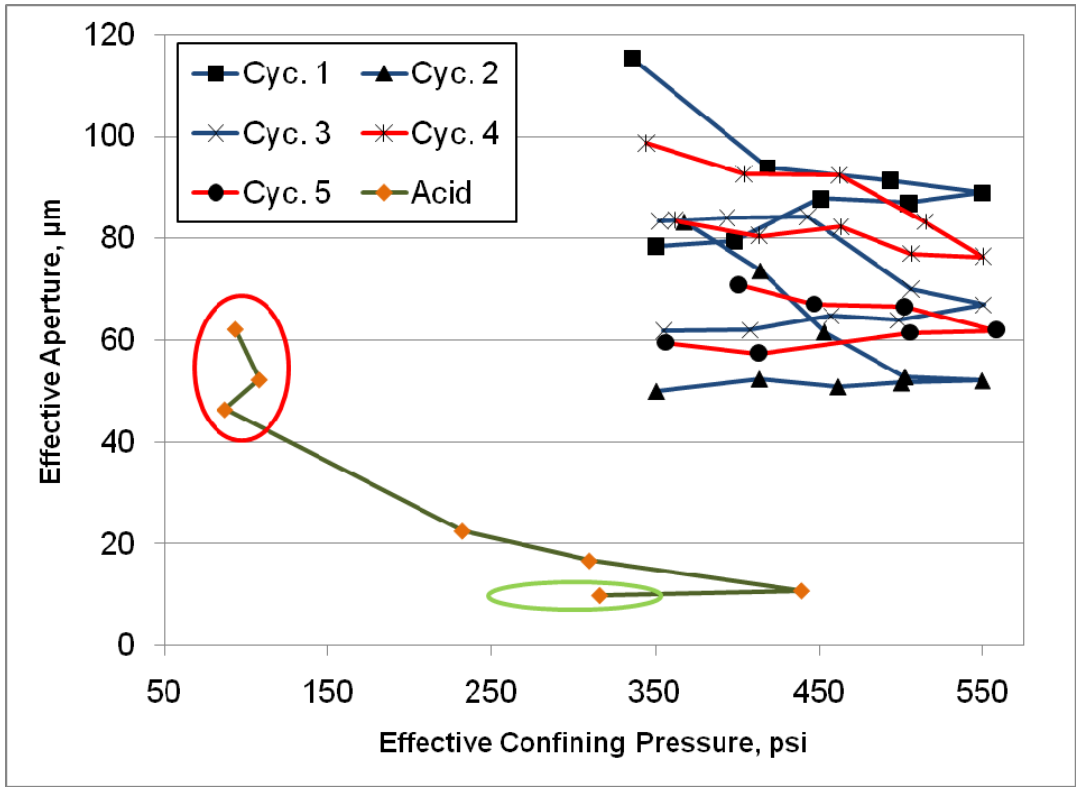


Fig. 4.5 – The aperture to confining pressure relationship for sample F14B. The baseline cycles are plotted as Cyc. 1-5 and the loading cycle after the core was acidified is plotted as Acid. The acidified core behaves quite differently from the baseline study. While the acidified core starts out with an aperture comparable to those seen in the baseline study it quickly drops to a value much below those seen in the baseline cycles.

CHAPTER 5 – CONCLUSIONS

A significant risk for geologic CO₂ storage is the leakage through existing wellbores in overlying formations. Significant leakage is likely to occur through conductive pathways within the cemented annulus, rather than through the matrix of cement. For such pathways, the coupling between geomechanics, geochemistry and the pathway geometry is important in assessing the potential leakage flux.

Using sustained casing pressure as an analog to CO₂ leakage along a wellbore we can get an estimate of the conductive pathway size. For the handful of wells studied to date have effective permeability values from tenths to a hundred mD (Table 2.3). As these values are orders of magnitude higher than the permeability of typical oil field cement, the flow path is best described in terms of an explicit geometry, e.g. a micro annulus, and not in terms of a permeable material. For CO₂ sequestration this insight is particularly important because coupling between geomechanics, geochemistry and leakage rate will depend strongly on the geometry of the leakage path. Further case studies might allow correlating the magnitude of pathway conductivity with a key parameter of the well, such as onset of leak or type of completion. Ideally it would be useful to study sustained casing pressure from a field scale, to look at the possible effect of cross flow between formations, sometimes seen as pressure buildup onset at one annulus after another well has reached a certain threshold. The development of a more complex model to study sustained casing pressure might be required to model several wells. This model should be flexible and robust enough to treat the physical properties of carbon dioxide as it will be immediately useful to estimating project scale leakage risk.

Laboratory experiments allow us to study the relation between geomechanics, geochemistry, and flow through a discrete pathway. Using cement cores with a realistic fracture and core flow equipment we were able to estimate fracture aperture from measured flow rates and pressure drops. We found that fracture apertures around 10 μm to 50 μm worked well in the equipment and matched both our SCP results and literature values for pathway size. We showed that after “strain hardening” the sample there is a reproducible relation between confining stress and fracture aperture size. This relationship is a function of the fracture geometry (asperity shape and distribution) and of the cement’s mechanical strength along the fracture. Uniform reaction along the fracture faces decreased the mechanical strength of cement, resulting in a smaller fracture aperture for a given confining stress when compared to the unreacted value. Our initial experiments lead to the hypothesis that a sufficiently degraded fracture might become self-sealing when under confining stress. Further experiments showed that the depth of alteration along the fracture surfaces might control how much smaller the aperture becomes at a given confining stress. The geometry of the fracture faces, i.e. the shape and size of the contacting asperities, might also be a factor as broader asperities would require more reaction before a significant change to their mechanical strength would occur. Further study to quantify under what conditions a fracture will close are warranted.

Future work

One feature of our previous work was that the chemical reaction was decoupled from the fluid flow and confining stress, but how might dynamic alteration of the fracture face affect the conductivity over time? Initial results (Fig. 5.1) indicate that reaction of acid with the cement fracture face is far from uniform and thus the long term behavior under stress will be more complex. Can the permeability of degraded cement be

measured and will a significantly altered cement plug or annulus allow CO₂ leakage? Additionally our work, to date, has used more reactive hydrochloric acid at ambient temperature. With more realistic down hole conditions and fluids (CO₂-saturated brine), the question arises as to whether the behavior will change in any other way besides in the time domain (e.g. precipitation of minerals or increase in degraded zone strength).

There remains much to be studied to estimate with any confidence well leakage risk and the long term fate of wells subject to CO₂ sequestration conditions. Additional case studies will allow us to create a larger matrix of possible effective leakage permeabilities and to tie them to higher order parameters, such as age of well or type of cement job. Many laboratory investigations remain, specifically, determining the conditions of self sealing under various geometries and with more accurate down hole conditions. While both methods have their merits only by combining results from analogs and laboratory studies will help to project long term leak of CO₂ from wells.

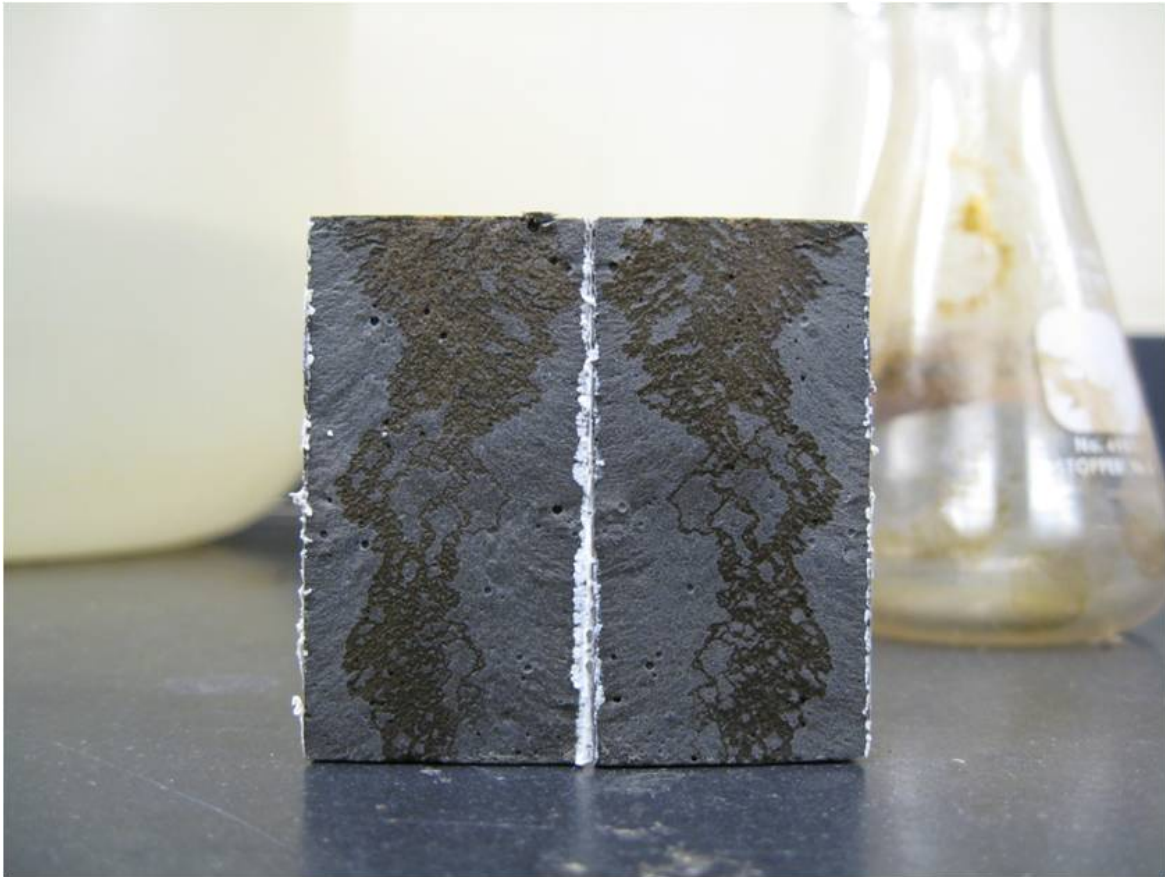


Fig. 5.1 – Initial results of flow through a fractured cement core using dilute hydrochloric acid. Note the channeling of flow through preferential pathways, which creates distinctly different reaction surfaces than we created with the uniform reaction technique.

REFERENCES

- Bourgoyne, A. T. Jr., S. L. Scott, W. Manowski. (2000) "A review of sustained casing pressure occurring on the OCS". Final Report, Contract No. 14-35-001-30749. Department of the Interior, Minerals Management Service.
- Boukhelifa, L., N. Moroni, S.G. James, S. Le Roy-Delage, M.J. Thiercelin, G. Lemaire. (2005) "Evaluation of cement systems for oil and gas-well zonal isolation in a full-scale annular geometry". SPE Drilling & Completion. March 2005. SPE 87195.
- Carey, J. W., M. Wigand, S. Chipera, G. WoldeGabriel, R. Pawar, P. Lichtner, S. Wehner, M. Raines, G. Guthrie. (2006) "Analysis and performance of oil well cement with 30 years of CO₂ exposure from the SACROC unit, West Texas, USA". 8th International Conference on Greenhouse Gas Control Technologies, Trondheim, Norway, Elsevier.
- Dusseault, M. B., M. N. Gray, P.A. Nawrocki. (2000) "Why oilwells leak: Cement behavior and long-term consequences". Society of Petroleum Engineers. SPE International Oil and Gas Conference and Exhibition. Beijing, China. 7 – 11 November, 2000. SPE 64733.
- Glasser, F. P., J. Marchand, E. Samson. (2008) "Durability of concrete - Degradation phenomena involving detrimental chemical reactions". Cement and Concrete Research **38**: 226-246.
- Gray, K.E., E. Podnos, E. Becker. (2007) "Finite element studies of near-wellbore region during cementing operations: Part I". Society of Petroleum Engineers. 2007 SPE Production and Operations Symposium. Oklahoma City, Oklahoma, USA. 31 March – 3 April, 2007. SPE 106998.
- Huerta, N.J., S.L. Bryant, L. Conrad. (2008) "Cement core experiments with a conductive leakage pathway, under confining stress and alteration of cement's mechanical properties via a reactive fluid, as an analog for CO₂ leakage scenario". Society of Petroleum Engineers. 2008 SPE Improved Oil Recovery Symposium. Tulsa, Oklahoma, USA. 19 – 23 April, 2008. SPE 113375.
- Huerta, N.J., S.L. Bryant, B.R. Strazisar, B.G. Kutchko, L.C. Conrad. (2009) "The influence of confining stress and chemical alteration on conductive pathways within wellbore cement". Energy Procedia **1**: 3571-3578.
- Huerta, N.J., D.A. Checkai, S.L. Bryant. (2009) "Utilizing sustained casing pressure analog to provide parameters to study CO₂ leakage rates along a wellbore".

- Society of Petroleum Engineers. 2009 SPE International Conference on CO₂ Capture, Storage, and Utilization. San Diego, California, USA. 2 – 4 November, 2009. SPE 126700.
- Iwai, K. (1976) “Fundamental studies of fluid flow through a simple fracture”. University of California at Berkeley. Doctoral Dissertation.
- James, S., L. Boukhelifa (2006) "Zonal isolation modeling and measurements - Past myths and today's realities". Society of Petroleum Engineers. 2006 Abu Dhabi International Petroleum Exhibition and Conference. Abu Dhabi, U.A.E. 5 – 8 November, 2006. SPE 101310.
- Jutten, J.J., A.J. Hayman. (1993) “Microannulus effect on cementation logs: Experiments and case histories”. Society of Petroleum Engineers. SPE Asia Pacific Oil & Gas Conference & Exhibition. Singapore. 8 – 10 February, 1993. SPE 25377.
- Kutasov, I.M. (1988) “Empirical correlation determined downhole mud density”. Oil & Gas Journal. December 12, 1988.
- Kutchko, B.G., B.R. Strazisar, D.D. Dzombak, G.V. Lowry, N. Thaulow. (2007) “Degradation of well cement by CO₂ under geologic sequestration conditions”. Environ. Sci. Technol. **41**: 4787-4792.
- Kutchko, B.G., B.R. Strazisar, D.D. Dzombak, G.V. Lowry, N. Thaulow. (2008) "Rate of CO₂ attack on hydrated class H well cement under geological sequestration conditions". Environ. Sci. Technol. **42**: 6237-6242.
- McCain, W.D. Jr., (1990) The Properties of Petroleum Fluids. 2nd Ed. PennWell. Tulsa, Oklahoma, USA.
- Mueller, D.T., V. GoBoncan, R.L. Dillenbeck, T. Heinold. (2004) "Characterizing casing-cement-formation interactions under stress conditions: Impact on long-term zonal isolation". Society of Petroleum Engineers. SPE Annual Technical Conference and Exhibition. Houston, Texas, USA. 26 – 29 September, 2004. SPE 90450.
- Nasr-El-Din, H.A., A. Al-Yami, A. Al-Aamri. (2007) "A study of acid cement reactions using the rotating disk apparatus". Society of Petroleum Engineers. 2007 SPE International Symposium on Oilfield Chemistry. Houston, Texas, USA. 28 February – 2 March, 2007. SPE 106433.
- Nelson, E.B., D. Guillot, Eds. (2006) Well Cementing. 2nd Ed. Schlumberger. Sugar Land, Texas, USA.
- Nicot, J.-P., K.P. Saripalli, S.D. Hovorka, S. Lakshminarasimhan. (2006) “Leakage pathways from potential CO₂ storage sites in the Texas Gulf Coast and

- implications for permitting”. Department of Energy, National Energy Technology Lab. 5th Annual Conference on Carbon Capture and Sequestration. Pittsburgh, Pennsylvania, USA. 8 – 11 May, 2006.
- Nordbotten, J.M., M.A. Celia, S. Bachu, H.K. Dahle, (2005) “Semianalytical solution for CO₂ leakage through an abandoned well”. Environ. Sci. Technol. **39**: 602-611.
- Onan, D.D. (1984) "Effects of supercritical carbon dioxide on well cements". Society of Petroleum Engineers. 1984 Permian Basin Oil & Gas Recovery Conference. Midland, Texas, USA. 8 – 9 March, 1984. SPE 12593.
- Pedam, S.K. (2007) “Determining strength parameters of oil well cement”. University of Texas at Austin. Masters Thesis.
- Reddy, B.R., Y. Xu, K. Ravi, D. Gray, P.D. Pattillo. (2007) "Cement shrinkage measurement in oilwell cementing - A comparative study of laboratory methods and procedures". Society of Petroleum Engineers. 2007 SPE Rocky Mountain Oil & Gas Technology Symposium. Denver, Colorado, USA. 16 – 18 April, 2007. SPE 103610.
- Shen, J.C., D.S. Pye. (1989) "Effects of CO₂ attack on cement in high-temperature applications". Society of Petroleum Engineers. 1989 SPE/IADC Drilling Conference. New Orleans, Louisiana, USA. 28 February – 3 March, 1989. SPE 18618.
- Tsang, Y.W., P.A. Witherspoon. (1981) "Hydromechanical behavior of a deformable rock fracture subject to normal stress". Journal of Geophysical Research **86**: 9287-9298.
- Tsang, Y.W., P.A. Witherspoon. (1983) "The dependence of fracture mechanical and fluid flow properties on fracture roughness and sample size". Journal of Geophysical Research **88**: 2359-2366.
- Watson, T.L., S. Bachu. (2007) “Evaluation of the potential for gas and CO₂ leakage along wellbores”. Society of Petroleum Engineers. 2007 SPE E&P Environmental and Safety Conference. Galveston, Texas, USA. 5 – 7 March, 2007. SPE 106817.
- Watson, T.L., S. Bachu. (2008) “Identification of wells with high CO₂-leakage potential in mature oil fields developed for CO₂-enhanced oil recovery”. Society of Petroleum Engineers. 2008 SPE/DOE Improved Oil Recovery Symposium. Tulsa, Oklahoma, USA. 19 – 23 April, 2008. SPE 112924.
- Witherspoon, P.A., J.S.Y. Wang, K. Iwai, J.E. Gale. (1980) "Validity of cubic law for fluid flow in a deformable rock fracture". Water Resources Research **16**: 1016-1024.

- Wojtanowicz, A.K., S. Nishikawa, R. Xu. (2001) "Diagnosis and remediation of sustained casing pressure in wells". Final Report. Department of the Interior, Minerals Management Service.
- Xu, R., A.K. Wojtanowicz. (2001) "Diagnosis of sustained casing pressure from bleed-off/buildup testing patterns". Society of Petroleum Engineers. SPE Production and Operations Symposium. Oklahoma City, Oklahoma, USA. 24 – 27 March, 2001. SPE 67194.
- Xu, R. (2002) "Analysis of diagnostic testing of sustained casing pressure in wells". Louisiana State University. Doctoral Dissertation.